REPORT DOCUMENTATION PAGE

Form Approved
OMB No. 0704-0188

1. AGENCY USE ONLY (Leave blank)	2. REPORT DATE	3. REPORT TYPE AND DATES COVERED
	December 1997	February 1, 1995–June 30, 1997

4. TITLE AND SUBTITLE
"Third and Seventh Harmonic Free Electron Laser Coherent Millimeter Radiation, and Studies of Short-Pulse Emission from FEL"

5. FUNDING NUMBERS

6. AUTHOR(S)
T.C. Marshall

7. PERFORMING ORGANIZATION NAME(S) AND ADDRESS(ES)
Department of Applied Physics
Columbia University
New York, NY 10027

8. PERFORMING ORGANIZATION REPORT NUMBER
Plasma Laboratory Report #134

9. SPONSORING/MONITORING AGENCY NAME(S) AND ADDRESS(ES)
Office of Naval Research, Physics Division
800 N. Quincy Street
Arlington, WA 22217-5660

10. SPONSORING/MONITORING AGENCY REPORT NUMBER

11. SUPPLEMENTARY NOTES

12a. DISTRIBUTION/AVAILABILITY STATEMENT
Approved for public release- distribution unlimited

12b. DISTRIBUTION CODE

13. ABSTRACT (Maximum 200 words)

Two and one-half years' research at the Columbia Free Electron Laser facility are are are summarized with an introductory overview followed by a selection of key reprints. Topics include: Short pulse high power millimeter emission using the Cerenkov effect in a dielectric-loaded waveguide, and coherent phase-reference harmonic radiation from a waveguide FEL. The latter is an experimental demonstration, while the first two topics are theoretical studies.

14. SUBJECT TERMS
Free Electron Laser Radiation

17. SECURITY CLASSIFICATION OF REPORT	18. SECURITY CLASSIFICATION OF THIS PAGE	19. SECURITY CLASSIFICATION OF ABSTRACT	20. LIMITATION OF ABSTRACT
Unclassified	Unclassified	Unclassified	

INTRODUCTION

This report is a summary of the principal research findings completed under grants N00014-95-1-0253 (February 2 1995 to January 31, 1996) and its follow-on, N00014-96-1-1136 (August 1 1996 to June 30, 1997), on experimental and theoretical research on Free Electron Lasers. In this two and one-half year period, work was completed on a thesis project involving the generation of FEL harmonic radiation, and additional work was done on the theory of short-pulse operation of the FEL. A more recent study, involving the production of Cerenkov radiation from short pulses of high energy electrons, was partly supported by this research as well. The major accomplishments of this projects are given here as reprints in the next three sections.

Section I consists of a paper showing how a 50psec pulse of high intensity millimeter radiation (wavelength = 1.5mm, 3GW/cm^2) could be produced from a 750kV electron beam; it was presented in SPIE section on intense microwave pulses at San Diego in July 1995, and is published in the SPIE Volume 2555, p. 250. This work is an outgrowth of work done on short-pulse FEL amplifiers that was begun with support from the preceding ONR grant, and which is described in publications reproduced in the final technical report (Columbia Plasma Laboratory report #128, 1995).

Section II is a preprint of a paper that has been accepted for publication in the IEEE Transactions on Plasma Science, special issue on high power microwave generation (to be published, 1998). The paper describes a source which can generate MW level pulses of psec broadband microwave radiation, using a pulsed electron beam having 6MeV energy.

Section III is a reprint of a paper published in Physical Review E summarizing our findings on a special type of harmonic FEL radiation; it also appeared in earlier versions in the Nuclear Instruments and Methods volumes relating to the FEL meetings in the summers of 1996 and 1995 (Rome, and New York City meetings respectively), as well as in the Beams '96 Conference held in Prague. We reproduce the Physical Review paper, as it is the latest and most comprehensive version. This work is an outgrowth of our interest in FEL harmonic radiations which dates from 1991. We use a "waveguide FEL" which is driven by a magnetron at its lower frequency "intersection" (unstable root) at 24Ghz, and which is configured as a travelling wave amplifier. This radiation bunches the beam at this frequency, and its harmonics. The bunch harmonics are arranged to couple to the third harmonic resonant FEL interaction (high frequency

"intersection") at 72Ghz, and we find a certain amount of power there that is coherent with the low frequency source. A more unusual finding is the non-resonant excitation of the seventh harmonic of the 24Ghz source, which generated appreciable amounts of power. This occurs because the bunched beam harmonic source currents travel at the same speed as the seventh harmonic TE_{72} wave..... an artifact of cylindrical geometry and Bessel function roots. To excite the seventh harmonic, the electron beam must be displaced off-axis. These phenomena were studied using a 1D FEL slippage two-frequency theory; the results were checked by others using a 3D theory. Thus we have demonstrated new mechanisms for generating coherent, phase-stable radiations at millimeter wavelengths using the FEL. It is worth noting, that another group has recently reported very tight bunching of a beam at the lower intersection frequency, with substantial harmonic content [Physical Review Letters 79, 3905 (1997)].

The project supported the part-time work of a visiting scholar (Dr. T-B. Zhang), Professor T.C. Marshall, and a full-time graduate research assistant, who was graduated with the PhD. in June, 1997.

I.

Narrow high power microwave pulses from a free electron laser

T. C. Marshall and T. B. Zhang

Department of Applied Physics, Columbia University,
New York, New York 10027

ABSTRACT

We have explored high power microwave ($\lambda = 1.5$mm) pulse amplification along a tapered undulator FEL using the 1D Compton FEL equations with slippage. For an appropriate taper, sideband instabilities are suppressed and a short (~50psec) Gaussian pulse will propagate in a nearly self-similar way as it grows in power, slipping through a much longer electron pulse (beam energy, 750kV; current, 100A; radius = 2mm; length = 200 radiation periods). This is in contrast to the example of pulse propagation in a constant parameter undulator, where the Gaussian pulse breaks up into irregularities identified with sidebanding. Variation of initial pulse width shows convergence to a 50psec wide output pulse. Because of the slippage of the radiation pulse through the electron pulse, the peak microwave pulse intensity, ~3GW/cm2, is about three times the kinetic energy density of the electron beam.

Keywords: short pulse, millimeter waves, free electron laser, high power

---

This paper studies a numerical model of a traveling wave, high gain, Compton FEL which operates at nearly optimal efficiency using a variable-parameter ("tapered") undulator and which produces an intense "clean" output spike pulse with a smooth spectrum almost free of sidebands. The hardware would include a "seed" source which supplies a suitable pulse having a Gaussian shape, as input to a high efficiency FEL traveling wave amplifier having an appropriately tapered undulator. Our findings are that one might expect to develop a millimeter wavelength FEL pulse having peak power ~3 GW/cm^2 and FWHM ~50 psec using a 0.75MeV, 100A electron beam. The powerful narrow pulse, about ten wavelengths wide, suggests potential application in the area of impulse radar.

Under certain conditions, the free electron laser [FEL] oscillator has been found to provide an output of narrow, chaotic high power "spike" pulses of radiation characterized by a wide irregular spectrum [1-3]. Furthermore, in the operation of a FEL oscillator, experiment [4] as well as numerical theory which carries the analysis well into the nonlinear regime [5], shows that the FEL can operate in a mode characterized by low efficiency together with a narrow spectrum, or in a mode that has higher efficiency and a wide spectrum. The latter has to do with the sideband instability [6] which has been observed experimentally [7,8] and which is also found in connection with superradiant spiking studies [9-13] since both [14] arise from slippage. However, there is also evidence that the sideband instability can be stabilized with an appropriately chosen taper of the undulator [15-17]. We therefore investigate the use of a tapered undulator to produce both a high power pulse as well as one that is narrow and regular in shape.

We now develop a numerical model which establishes how such a FEL pulse can be prepared; we study a short millimeter wave pulse which is propagating along a much longer pulse of electrons that is traversing an undulator [18]. At FEL resonance, as the light wave moves down one undulator period, it slips ahead of the electrons by one optical wavelength λ_s. We shall study the case where the electron beam pulse is much longer than the overall slippage distance $L_s = N_w \lambda_s$, so that essentially no radiation appears ahead of or behind the electron pulse. (A number of recent publications have considered the wealth of interesting effects which occur at the beginning and the end of the electron pulse, which involve "superradiance" [9-13].) We begin by studying a set of 1D equations which are appropriate for the Compton FEL:

$$\frac{\partial \gamma_j(x,y)}{\partial x} = -\frac{2\rho\gamma_r^2 A_s \sin\psi_j}{\gamma_j \beta_{j\parallel}} \tag{1}$$

$$\frac{\partial \theta_j(x,y)}{\partial x} = \frac{1}{2\rho}\left[1 - \frac{k_s(1-\beta_{j\parallel})}{k_w \beta_{j\parallel}}\right] \tag{2}$$

$$\frac{\partial A(x,y)}{\partial y} = i\gamma_r \left\langle \frac{e^{-i\theta}}{\gamma} \right\rangle \qquad (3)$$

The above equations are derived directly from the original 1D time-dependent FEL equations [6] by transforming the variables z and t into new independent variables x and y [9], i.e. $x = (ct - z)/l_c$, $y = (z - v_{||}t)/l_c\beta_{||}$; here, $l_c = \lambda_s/4\pi\rho$ is the cooperation length which is defined as the minimum distance over which an electron may interact cooperatively with the radiation [10], $\rho = \frac{1}{\gamma_r}\left(\frac{a_w\omega_p}{4ck_w}\right)^{2/3}$, is the Pierce parameter; $\beta_{j||} = \left[1 - (\mu^2 - 2a_w a_s \cos\psi_j)/\gamma_j^2\right]^{1/2}$ is the axial velocity of the jth electron, $\mu^2 = 1 + a_w^2 + a_s^2$, a_w and a_s are the normalized vector potentials of the undulator ($eB_\perp/k_w mc^2$) and radiation field ($eE_s/k_s mc^2$); γ_j is the relativistic factor of the jth electron, $\psi_j = \theta_j + \phi$ is the relative phase of the jth electron with respect to the radiation pulse, $A(x, y) = A_s e^{i\theta}$ is the complex amplitude of the radiation pulse with $A_s = \frac{1}{\sqrt{\gamma_r\rho}}\frac{\omega_s}{\omega_p}a_s$, and ϕ is the phase shift of the radiation pulse. The angular brackets in the right-hand side of equation (3) indicate an ensemble average over all electrons. For the other quantities: γ_r is the resonant energy of electron in units of mc^2, $k_w = 2\pi/l_w$ is the wave number of the undulator, l_w is the undulator period; $k_s = 2\pi/\lambda_s = \omega_s/c$ is the wave number of the radiation pulse, λ_s is the radiation wavelength, l_w and λ_s satisfy the resonance condition $\lambda_s = \frac{l_w\left(1 + a_w^2\right)}{2\gamma_r^2}$, $\omega_p = \left(\frac{4\pi e^2 n_e}{m}\right)^{1/2}$ is the plasma frequency for n_e electrons/cm^3. The original FEL wave equations have been obtained assuming the field amplitude is a slowly varying function of time; this approximation has been verified in the application for the short pulse propagation discussed here. The operation of the FEL described here is on the borderline between the Compton and Raman regimes, and if an actual device is to be constructed, the beam space charge effects should be included to insure accuracy; however, for this illustrative example, we have not incorporated this complication, nor that of an overmoded waveguide, an essential element to contain the waves; both items are comparatively straightforward to include in the above equations. From the 1D formulation we shall obtain the output wave intensity, namely the power normalized to the cross section of the electron beam.

The numerical simulation is based on the computational model described by equations (1) to (3). The FEL works as a traveling wave amplifier. The spatial distribution of simulation electrons has a rectangular profile, the electrons are taken to be monoenergetic, and at the undulator entrance, they are uniformly distributed inside the beam length L_b with one thousand simulation electrons per radiation wavelength. For each wavelength-size "strip" of electrons, the relative phase location of the electrons with respect to the radiation field is uniformly distributed from $-\pi$ to π. The input radiation pulse is "seeded" inside the electron beam, with its initial amplitude $a_{s0} = 10^{-4}$ (9 kW/cm^2 at 1.5mm wavelength). The pulse profile and width can be varied so that we can study the evolution of various pulses. For the output format of the computational results, the electron beam pulse and the radiation spike are plotted as the function of independent variables x and y respectively, which implies two moving "windows" with the former at the speed of light c and the latter at the speed of electrons $v_{||}$, both are scaled in the units of the radiation wavelength λ_s from their leading edge. Since all these quantities are recorded at various undulator positions, these results will describe the time evolution of the pulses. In several test runs, we have carried out simulations for different FEL parameters, including different lengths of beam pulses and radiation pulses. Our results for "superradiant" pulse evolution are in a very good agreement with that of previous authors[9] and provide a calibration of our code.

Our main interest is to investigate an initial short radiation pulse propagating through a sufficiently long electron pulse. The initial radiation pulse has a Gaussian profile and is injected into the rear part of the electron beam pulse; the

peak of the initial pulse is located at $y = 170\ \lambda s$. The radiation pulse starts from that position at the undulator entrance, and then moves toward the front of the electron pulse as it moves along the undulator. The Fourier-transformed spectrum is also Gaussian and has a central frequency $\omega_S = 1.26 \times 10^{12}\ sec^{-1}$. Other simulation parameters of the FEL amplifier are listed in Table I, where a representative electron beam pulse length of 30cm (~1nsec) is taken; this beam pulse is 200 wavelengths long, and so the optical pulse moves only halfway through as it traverses 100 undulator periods.

Table I. Simulation parameters of radiation spike propagating in electron beam pulse

Beam parameters	
Electron beam energy	$\gamma = 2.5$
Electron beam current	$I_b = 100$ (A)
Beam intensity	$0.63 GW/cm^2$
Electron beam radius	$r_b = 0.2$ (cm)
Beam pulse length	$L_b = 200\ \lambda_S$ (30cm)
Undulator parameters	
Undulator period	$l_w = 1.5 - 1.1$ (cm); linear ramp
Undulator taper	$\eta = 2 \times 10^{-3}\ (cm^{-1})$
Undulator parameter	$a_w = 0.2$ (constant)
Undulator length	$N_w = 100$
Radiation pulse	
Radiation wavelength	$\lambda_S = 1.5$ (mm)
Spike length(FWHM, intensity)	$L_r = 10\lambda_S$
Initial pulse amplitude	$a_{S0} = 10^{-4}$ ($9\ kW/cm^2$)
Peak spike amplitude	$a_S = 0.06$ ($3 GW/cm^2$)
Other parameters	
Pierce parameter	$\rho = 0.023$
Cooperation length	$lc = 4\ \lambda_S$

Figure 1 shows the pulse evolution in a constant period undulator ($l_w = 1.5$cm. at four undulator positions $N_w = 0, 25, 50$ and 100. In these figures, the electron envelope is at rest and the optical spike propagates from the right to left as N_w increases. The radiation spike retains the initial profile until approximately 50 undulator periods where the growth becomes saturated. Saturation occurs when the loss of beam energy causes the interaction to drop out of resonance. Examining the spectrum of the pulse at $N_w = 100$ (see right side of Figure 3), we find the spectrum has developed prominant sidebands; these become comparable to the carrier power by 150 periods.

If the undulator is tapered, we expect the growth of the sideband can be suppressed, and in Figure 2 we show the results. The undulator period is linearly tapered from1.5cm to 1.05cm in 150 periods. All other conditions are the same as in Figure 1 and are obtained from Table I. In this numerical experiment, we did not optimize the undulator taper to pursue the highest efficiency enhancement: instead, the appropriate taper was chosen for the purposes of obtaining the "cleanest" pulse (however, this optimized taper is not very different from the taper which extracts maximum energy from the beam). Unlike the untapered case, the radiation pulse at high amplitude does not radically change its shape, but displays a narrow, regular profile throughout the slippage region. The width of the initial Gaussian pulse is FWHM $\sim 10\lambda_S$ in intensity; it grows in amplitude and broadens during the first 25 periods; it continues to grow while keeping a nearly regular profile as it narrows in width between 50 and 100 periods. We have tried various widths of the initial Gaussian pulse, as well as a different initial amplitude profile varying as $\sim 1/\cosh(\alpha y)$ (a solitary wave solution [19]), and we find the variation of initial choices converges to a similar output pulse profile and width, although the number of undulator periods needed to form the self-similar pulse profile may vary. This suggests that a short optical pulse may eventually evolve to a self-similar spike in the slippage region of the tapered undulator. The characteristic width of the spike is similar to the prediction of the Ginzburg-Landau solitary wave theory [20]. In the constant period undulator, the self-similar feature is lost when the FEL system goes out of resonance. Returning to Figure 3 (left side), we find not only a cleaner spectrum, but evidence of sideband suppression as well.

In Figure 4 we compare the cases of an untapered undulator (dotted line), a taper as given in the Table (solid line), and a steeper taper (dot-dash line), about 20% larger than that given in the Table. Examining the electron energy profile, we find considerable efficiency enhancement in the tapered undulators; however, the optimum taper yields not only a better pulse shape, but a higher peak power. The maximum value of the normalized field amplitude $a_S = 0.06$ ($\sim 3 GW/cm^2$) corresponds to an intensity higher than the beam kinetic energy intensity; this enhancement in power is caused by the slippage of the radiation pulse over "new" electrons as it moves down the undulator. The ragged profile of the electron energy in the constant undulator is found to smooth out in the tapered undulator. The strong intensity of the spike forms a very deep potential well which may trap most of the electrons even though they have an energy spread.

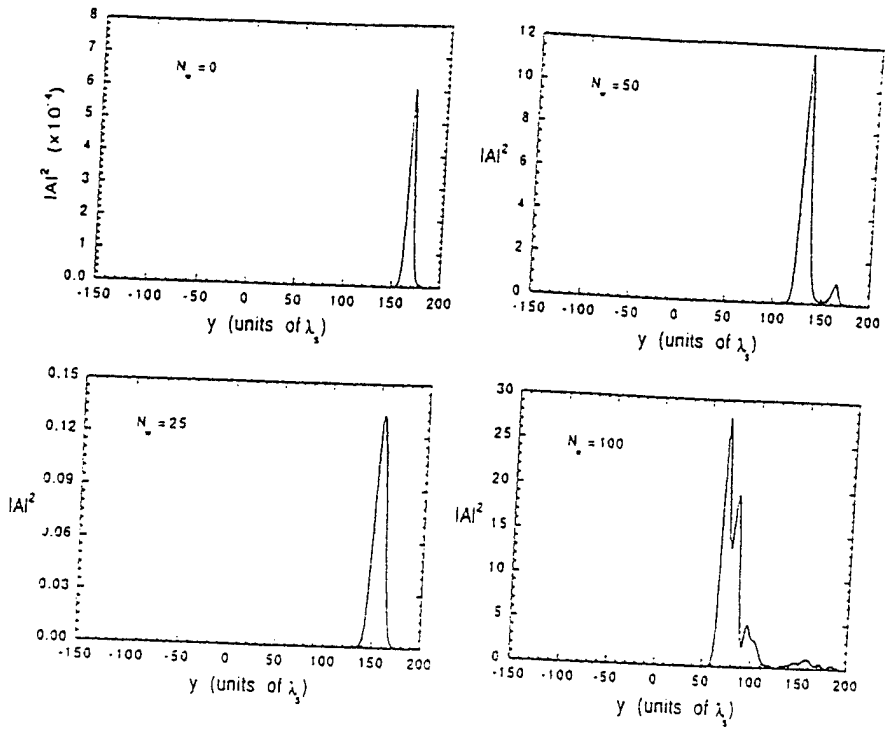

Figure 1. Constant undulator period simulation. The radiation pulse slips forward into the electron beam from right to left.

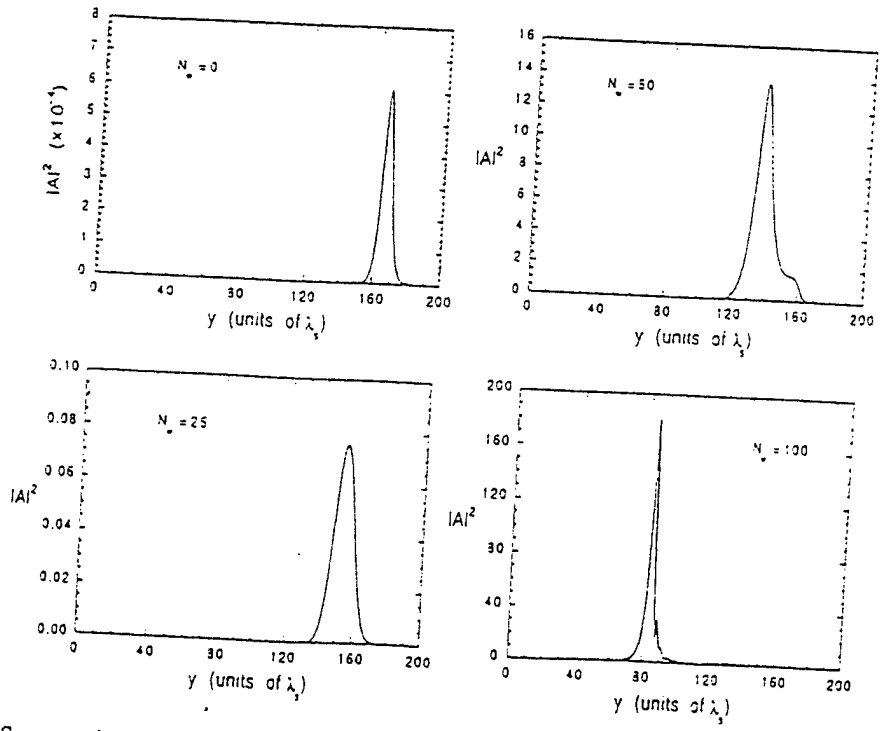

Figure 2. Same as in Figure 1 except that the undulator period is linearly tapered from 1.5 cm to 1.1 cm.

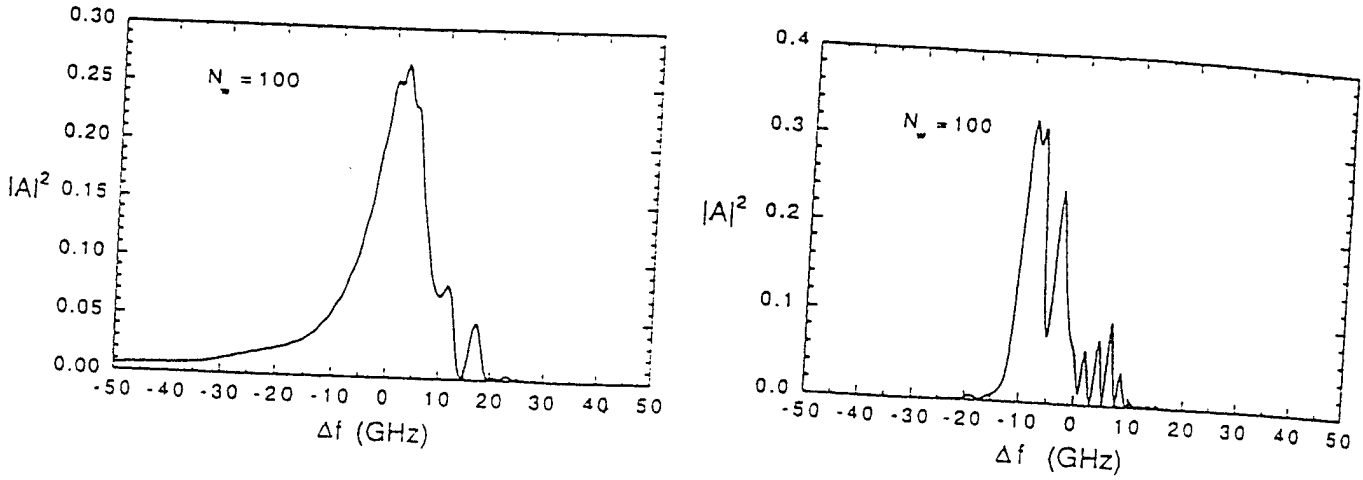

Figure 3. Spectrum of the pulse at 100 periods, tapered undulator (left) and untapered (right).

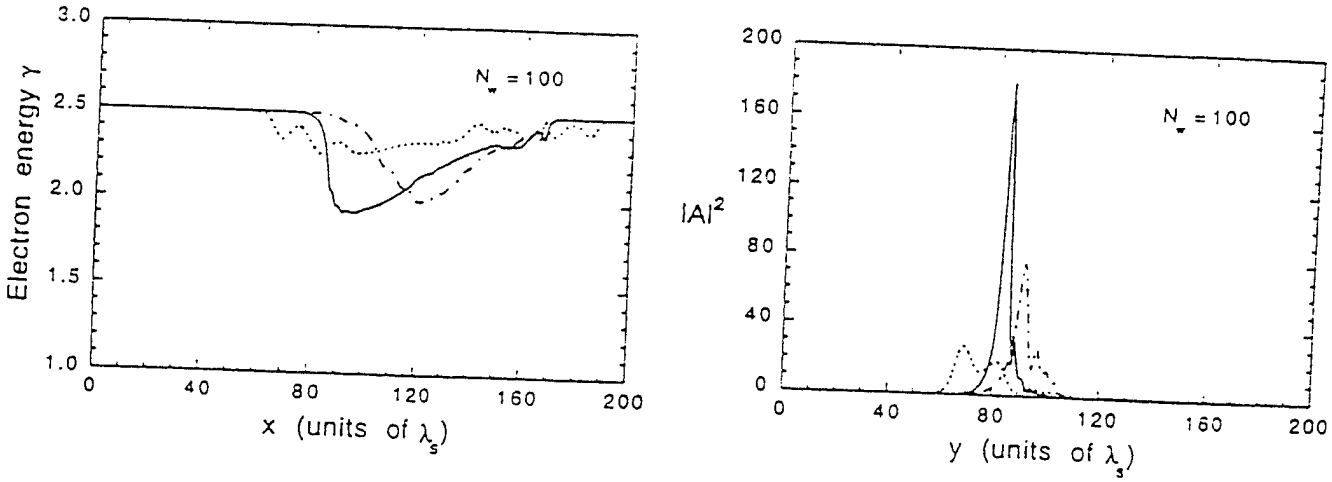

Figure 4. Electron energy profile (left) and pulse profile (right) for untapered undulator (dotted line); tapered undulator according to Table I (solid line); and a taper 20% larger yet (dash-dot line).

The choice of the 1.5mm wavelength was arbitrary although this is representative of FEL performance with the chosen beam parameters. (The same qualitative features were obtained in another tapered undulator FEL simulation for a much higher beam energy and wavelength of 8μm.[18]). The pulses are typically about 5-10 wavelengths FWHM, and so a 1.5mm FEL source produces a pulse width of roughly 50psec. Because of the large optical intensity achieved, one would not expect optical guiding to be effective beyond the region of exponential growth [21], so an overmoded waveguide should be used to guide the radiation along the electron beam.

The overall power gain of the spike pulse is ~50dB. This raises the question of noise, particularly electron random noise, and how it affects the amplified pulse. We have introduced particle noise [22] into the code and find that this can cause, under certain conditions, a "spiky" noise signal that both leads and trails the main pulse. Small energy present in the wings of the Gaussian pulse can be amplified under noisy conditions to high amplitude, and if there is sufficient gain, the noisy energy that precedes the main pulse will broaden the energy distribution of the electrons that this pulse will slip into, resulting in degraded amplifier performance. However, starting from our choice of initial power ~ 9kW/cm2, we find that particle noise has no effect on the output; but this is not true at much lower input levels, and the noise also becomes more important at shorter wavelengths (we have found that a steeper taper is useful to inhibit noise growth at short wavelength). The type of noise we have introduced into the simulation is Gaussian, and it should be noted that an electron beam in practice may have particle noise in excess of this.

In conclusion, we have found that injection of a single short radiation pulse into a long electron beam pulse at the input of a tapered undulator traveling wave FEL amplifier should result in the development of an intense spike which is comparatively "clean" in both time and frequency domains, and which propagates in a nearly self-similar way along the undulator. Because of the slippage, the peak pulse intensity is enhanced and may exceed the electron beam intensity. Since the pulse spectrum is regular, the output pulse from the FEL should be useful for technical applications.

ACKNOWLEDGEMENT

This work is sponsored by the Office of Naval Research and the Department of Energy.

REFERENCES

1. R. W. Warren, J. C. Goldstein and B. E. Newnam, *Nucl. Instrum. Methods*, Vol. A250, p. 19, 1986.
2. B. A. Richman, J. M. J. Madey and E. Szarmes, Phys. Rev. Lett., Vol. 63, p. 1682, 1989.
3. J. W. Dodd and T. C. Marshall, *IEEE Trans. Plasma Sci.*, Vol. PS-18, p. 447, 1990.
4. D. Iracane, V. Fontenay, P. Guimbal, S. Joly, S. Striby and D. Touati, *Phys. Rev. Lett.*, Vol. 72, p. 3985, 1994.
5. D. Iracane and J. L. Ferrier, *Phys. Rev. Lett.* , Vol. 66, pp. 33- , 1991.
6. N. M. Kroll, P. L. Morton and M. N. Rosenbluth, *IEEE J. Quantum Electron.* , Vol. QE-17, p. 1436, 1981.
7. R. W. Warren, B. E. Newnam and J. C. Goldstein, *IEEE J. Quantum Electron.* , Vol. QE-21, p. 882, 1985.
8. F. G. Yee, J. Masud, T. C. Marshall and S. P. Schlesinger, *Nucl. Instrum. Methods*, Vol. A259, p. 104, 1987.
9. R. Bonifacio, B. W. J. McNeil and P. Pierini, *Phys. Rev.* , Vol. A40, p. 4467, 1989.
10. R. Bonifacio, N. Piovella and B. W. J. McNeil, *Phys. Rev.* , Vol. A44, p. 3441, 1991.
11. W. M. Sharp, W. M. Fawley, S. S. Yu, A. M. Sessler, R. Bonifacio, and L. DeSalvo Souza, *Nucl. Instrum. Methods* Vol. A285, p. 217, 1989.
12. G. T. Moore and N. Piovella, *IEEE J. Quantum Electron.*, Vol. QE-27, p. 2522, 1991.
13. S. J. Hahn and J. K. Lee, *Phys. Rev.* , Vol. E48, p. 2162, 1993.
14. R. M. Caloi, *Phys. Rev.* , Vol. A46, p. 7934, 1992.
15. F. G. Yee, T. C. Marshall and S. P. Schlesinger, *IEEE Trans. Plasma Sci.*, Vol. PS-16, p. 162, 1988.
16. B. Hafizi, A. Ting, P. Sprangle, and C. M. Tang, *Phys Rev.* , Vol. A38, p. 197, 1988.
17. R. P. Pila and A. Bhattacharjee, *Phys. Plasmas*, Vol. 1, p. 390, 1994.
18. T. B. Zhang and T. C. Marshall, *Phys. Rev. Lett.* , Vol. 74, p. 916, 1995.
19. S.Y. Cai and A. Bhattacharjee, *Phys. Rev.* , Vol. A43, p. 6934, 1991.
20. Li-Yi Lin and T. C. Marshall, *Phys. Rev. Lett.* , Vol. 70, p. 2403, 1993.
21. E. T. Scharlemann, p. 291 in Laser Handbook Vol. 6, "Free Electron Lasers", W. Colson, C. Pellegrini, A. Renieri, editors, N. Holland, 1990.
22. C. Penman and B. W. J. McNeil, Opt. Commun., Vol. 90, p. 82, 1992.

II.

revised 10/9/97

A Cerenkov Source of High Power Picosecond Pulsed Microwaves

T-B. Zhang,* T.C. Marshall,† and J.L. Hirshfield#,*

*Omega-P, Inc., 202008 Yale Station, New Haven, CT 06520

†Department of Applied Physics, Columbia University, New York, NY 10027

#Department of Physics, Yale University, New Haven, CT 06511

ABSTRACT

One or more electron bunches passing along the axis of a dielectric-lined cylindrical waveguide are shown to emit picosecond pulses of high power broadband microwave radiation. The bunches can be generated by an S-band rf gun, and thus spaced from one another by 10.5 cm in a macropulse sequence; or a single more intense bunch can be generated using a laser-illuminated photocathode in the rf gun. Theory is developed for the excitation of TM_{0m} modes of this waveguide which propagate at the bunch velocity, from Cerenkov radiation emitted by a single intense bunch. A train of psec coherent wake-field pulses are shown to follow the bunch, when the waveguide modes have nearly constant spacing in frequency. An example is shown for an alumina-lined waveguide, with 10 nC, 3-15 psec bunches having an initial energy of 6 MeV. Computations are presented of the mode spectrum of the radiation and its time structure. It is also shown that measurements of the mode spectrum, or of the energy loss of the bunch, can be used to infer the axial density profile of the bunch. Certain features of the theory are compared with the results of a preliminary experiment.

I. Introduction

If high-energy electrons pass along a channel traversing a dielectric medium, coherent millimeter and microwave radiation can be produced by the Cerenkov effect, if the electron speed is greater than the phase velocity of the waves [1,2,3,4]. When the electrons are in a continuous beam, linearized analysis for the fields and the self-consistent motion of the particles leads to a dispersion relation which predicts exponential growth or decay of the waves. For the nonlinear regime of particle trapping, the phase relationship between the waves and the particles will either allow the extraction of energy from the electrons and emission of radiation, or the acceleration of the particles [5]. In previous analyses of this problem, the electron stream has been initially unbunched, and the radiation occurred at a discrete frequency given approximately by the intersection of the electron beam dispersion line ($\omega = \beta c k_z$) with the dielectric-loaded waveguide line. However, as we shall show in this paper, if the beam consists of a single short bunch of electrons, or a succession of such bunches, then many modes of the structure can be excited simultaneously. By proper choice of waveguide dimensions and dielectric constant, we find that these modes can be phased so as to constructively interfere, to produce a distinctive sharply-pulsed Cerenkov wake field which trails the particles as they move along the axis of the channel in the dielectric [6]. This Cerenkov wake field, which here is embodied in the TM_{0m} modes of the structure, has a short-pulse (psec) time signature and MW-level peak power for available experimental conditions. The efficiency of this high power microwave source depends on the waveguide geometry, length, bunch energy and bunch size. In the example discussed below, 20% of the electron bunch energy is converted into radiation for the parameters chosen; this percentage increases as the length of the interaction increases. Broadband psec microwave and millimeter wave radiation may have applications in remote sensing and spectroscopy. Conversely, measurements of the

radiated spectrum and/or bunch energy loss in a selected dielectric waveguide segment may be used to infer the axial bunch length.

In what follows, we analyze a system depicted in Fig. 1 which consists of the following elements. A thermonic or photoelectric cathode rf electron gun is taken as the source of the electron bunch or bunches. Such an rf gun is typically powered by a conventional microwave source (e.g., a klystron) which provides 5-10 MW of L- or S-band power. This gun will, at the crest of the rf field, emit pulses of electrons about 3-9 psec (1-3 mm) in length which are spaced apart by the rf period (10.5 cm for the S-band case). The energy of the electrons can be as high as 6 MeV for a 2-1/2 cell rf gun, as confirmed in experimental tests in the Yale Beam Physics Laboratory [7]. The S-Band source can be pulsed at up to several hundred Hz, with a macropulse length of several microseconds. The stream of electron pulses provided by this gun (with suitable downstream focusing elements) is directed down the axis of a hollow dielectric cylinder, with outer radius R and inner radius a , coated on its outside with a conducting layer. The waveguide modes of this structure which readily interact with the on-axis electrons are of the TM_{0m} class. For simplicity in what follows, we shall assume the waves to move only along the device in the direction of the electron flow; e.g., there is no counter-traveling wave from reflections. Spent electrons can be deflected and collected at the end of the system. The axial phase velocity of the waves nearly equals the speed of light, so the radiation presumably can be coupled into free space using a gentle uptaper in the inner and outer waveguide radii. However, discussion of this tapered waveguide and the resulting radiation pattern in free space is beyond the scope of this paper.

In Section II we present the wake field theory in such a cylindrical waveguide lined with a thick shell of alumina. Alumina has excellent vacuum and mechanical properties, a high relative dielectric constant (~9-10) and low loss. It is a ceramic which can be

fabricated into the geometry we have chosen, coated on its interior to avoid charge build-up, and metalized on its exterior to provide a good outer conducting wall. In Section III we present computational results under typical conditions for a single injected electron bunch having a charge of 10 nC, that will be seen to excite fields with up to 3.3 MW peak power. Wake field radial and axial electric field patterns, temporal power histories, and mode amplitudes are presented. It is pointed out that measurement of the mode spectrum can be used to infer the axial bunch profile, and that measurement of the energy loss of a bunch can be used to infer the effective bunch length. In Section IV we describe a preliminary experiment in which a spectrum of modes was excited in a dielectric-lined cylindrical waveguide, using a 600 keV unbunched beam; the observed mode frequencies are compared with frequencies calculated using the theory given in Section II. In Section V results of the work are summarized.

II. Wakefield theory and radiation modes

The model analyzed here is a cylindrical waveguide, consisting of dielectric material with an axisymmetric hole; the outer surface of the cylinder is coated with a low-loss conductor. The dielectric constant κ is assumed to be independent of frequency. The geometry is depicted in Fig. 1. Electrons are injected along the z-axis in discrete axisymmetric bunches, with charge density given by $\rho(r,z,t) = -(Ne/2\pi r)\,\delta(r) f(z-vt)$, where e is the magnitude of the electron charge; N is the total charge number in the bunch; $\delta(r)$ is the transverse charge distribution, assumed to be of infinitesimal width in r; and $f(z-vt)$ is the longitudinal charge distribution for bunch particles moving at axial speed v. For this geometry, axisymmetric orthonormal wave functions can be found for the electromagnetic fields that separate into *TE* and *TM* classes. Only the *TM*-modes have an axial electric field; these are the modes considered here. Non-axisymmetric modes do not separate into *TE* and *TM* classes. For the geometry shown in Fig. 1, conditions

can be found where all *TM* modes have phase velocities equal to v, corresponding to wakefields that move in synchronism with the electron bunches. The field components for the complete orthonormal *TM* mode set are given by

$$E_z(r,z,t) = \sum_{m=0}^{\infty} E_m \frac{f_m(r)}{\alpha_m} e^{-i\omega_m z_o/v}, \tag{1}$$

where

$$f_m(r) = \frac{1}{P_0(k_{2m},R,a)} \begin{cases} P_0(k_{2m},R,a)\, I_0(k_{1m}r), & 0 \le r \le a \\ P_0(k_{2m},R,r)\, I_0(k_{1m}a), & a \le r \le R \end{cases}, \tag{2}$$

and $z_o = z - vt$;

$$E_r(r,z,t) = i \sum_{m=0}^{\infty} E_m \frac{g_m(r)}{\alpha_m} e^{-i\omega_m z_o/v}, \tag{3}$$

where

$$g_m(r) = \frac{1}{P_0(k_{2m},R,a)} \begin{cases} \gamma\ P_0(k_{2m},R,a)\, I_1(k_{1m}r), & 0 \le r \le a \\ \gamma_\kappa P_1(k_{2m},R,r)\, I_0(k_{1m}a), & a \le r \le R \end{cases}; \tag{4}$$

and

$$H_\theta(r,z,t) = c\beta\, E_r(r,z,t) \begin{cases} 1, & 0 \le r \le a \\ \kappa, & a \le r \le R \end{cases}. \tag{5}$$

As we will see later, the field amplitude E_m is expressed by the product of the Coulomb field and a structure factor that depends on the electron bunch size. In the above equations, $P_0(k,R,r) = J_0(kR)N_0(kr) - J_0(kr)N_0(kR)$ and $P_1(k,R,r) = J_0(kR)N_1(kr) - J_1(kr)N_0(kR)$; $J_m(x)$ and $N_m(x)$ are m-th order Bessel functions of the first and second kinds, and $I_m(x)$ is the modified Bessel function; a and R are radii of the central vacuum hole and the outer waveguide wall, respectively. The normalizing constant is found to be

$$\alpha_m = \frac{1}{2}\left\{\frac{1}{\kappa}\left(\frac{\gamma}{\gamma_\kappa}\right)^2 I_1^2(k_{1m}a)\left[\left(\frac{R}{a}\right)^2\left(\frac{P_1(k_{2m},R,R)}{P_1(k_{2m},R,a)}\right)^2 - 1\right] - (\kappa-1)I_0^2(k_{1m}a) - I_1^2(k_{1m}a)\right\};$$

where $\beta = v/c$; $\gamma = \left(1-\beta^2\right)^{-1/2}$; and $\gamma_k = \left(\kappa\beta^2 - 1\right)^{-1/2}$. The (evanescent) transverse wave number in the vacuum is k_{1m}; the (real) transverse wave number in the dielectric is k_{2m}, and $k_{1m} = \omega_m/c\beta\gamma = k_{2m}\gamma_\kappa/\gamma$. The eigenfrequencies are $\omega_m = c\beta\gamma k_{1m} = c\beta\gamma_\kappa k_{2m}$. Since all *TM* modes have phase velocities equal to v, we also have $\omega_m = c\beta k_{z,m}$. For the fields given by Eqs. 1-5, ortho-normalization obtains in the form

$$\int_0^R dr\, r\, E_{z,m} D_{z,n}^* = \delta_{mn}\frac{a^2}{\sqrt{\alpha_m\alpha_n}}\varepsilon_o E_m E_n \exp\left[-iz_o(\omega_m - \omega_n)/v\right], \tag{6}$$

where $D_{z,n}^* = \varepsilon E_{z,n}^* = \kappa\varepsilon_o E_{z,n}^*$ in the dielectric, and $D_{z,n}^* = \varepsilon_o E_{z,n}^*$ in the vacuum hole. The dispersion relation is found to be

$$\frac{I_1(k_1a)}{I_0(k_1a)} = \frac{\kappa k_1}{k_2}\frac{J_0(k_2R)N_1(k_2a) - J_1(k_2a)N_0(k_2R)}{J_0(k_2R)N_0(k_2a) - J_0(k_2a)N_0(k_2R)}. \tag{7}$$

It is noted that one can have eigenfrequencies with nearly periodic spacing, since $k_{2m}(R-a) \to (n+1/2)\pi$ as $\kappa \to \infty$. As $m \to \infty$ the asymptotic eigenfrequency spacing approaches $\Delta\omega = \pi c\beta\left[(R-a)\sqrt{\kappa\beta^2-1}\right]^{-1}$. The wake field is more strongly peaked and more closely periodic in z_o as the eigenfrequencies become more nearly periodic, i.e. as a higher value of κ is used.

To find wake fields induced by an electron bunch, one expands in orthonormal modes the solution of the inhomogeneous wave equation,

$$\left[\frac{1}{r}\frac{\partial}{\partial r}\left(r\frac{\partial}{\partial r}\right)+\frac{\partial^2}{\partial z^2}-\frac{\kappa(r)}{c^2}\frac{\partial^2}{\partial t^2}\right]E_z(r,z,t)=S_z(r,z,t), \tag{8}$$

with the source function $S_z(r,z,t)=\mu_o\frac{\partial j_z}{\partial t}+\frac{1}{\varepsilon_o}\frac{\partial \rho}{\partial z}$, where the z-component of the current density is $j_z(r,z,t)=v\rho(r,z,t)$, and where $S_z(r,z,t)=0$ for $r\geq a$. A complete solution can be constructed from fields as given in Eq. 1-5, since these are solutions of Eq. 8 with $S_z(r,z,t)=0$ everywhere. We expand the solution of Eq. 8 in the interval $0\leq r\leq R$ in a Fourier integral.

$$E_z(r,z,t)=\sum_{m=0}^{\infty}\frac{1}{\alpha_m}f_m(r)\int_{-\infty}^{\infty}dk\,A_m(k)\,e^{-ikz_o}. \tag{9}$$

Inserting Eq. 9 into Eq. 8, and multiplying both sides by $w(r)D^*_{z,n}(r,z,t)$ gives

$$A_m(k)=\frac{1}{2\pi\alpha_m\left(k^2-\omega_m^2/v^2\right)}\int_0^R r'\,dr'\int_{-\infty}^{\infty}dz'_o\,S_z(r',z'_o)\kappa(r')f_m(r')w(r')e^{ikz'_o} \tag{10}$$

where the weighting factor is $w(r)=\left[-\gamma^2,\gamma_\kappa^2\right]$ in the intervals $\left[(0\leq r\leq a),(a\leq r\leq R)\right]$, respectively. Then, integrating over k, with due regard for choice of the contour of integration consistent with causality, and invoking Eq. 6 yields

$$E_z(r,z,t)=\sum_{m=0}^{\infty}\int_0^R r'\,dr'\int_{-\infty}^{\infty}dz'_o\,S_z(r',z'_o)\,G_m(r,z_o;r',z'_o)\,, \tag{11}$$

where the Green's function $G_m(r,z_o;r',z'_o)$ is

$$G_m(r,z_o;r',z'_o)=\frac{-iv\kappa(r')}{2\omega_m\alpha_m a}w(r')f_m(r')f_m(r)e^{-i\omega_m|z_o-z'_o|/v}, \tag{12}$$

For a rectangular bunch $\rho(r,z,t) = -Ne(1/2\pi r)\delta(r)/\Delta z$ in the interval $z_o - \Delta z/2 \le z \le z_o + \Delta z/2$, and $\rho(r,z,t) = 0$ otherwise, one finds for the spontaneous wake field the result

$$E_z(r,z,t) = -E_o \sum_{m=0}^{\infty} \frac{f_m(r)}{\alpha_m} \frac{\sin(\omega_m \Delta z/2v)}{(\omega_m \Delta z/2v)} e^{-i\omega_m z_o/v}. \tag{13}$$

While for a Gaussian bunch $\rho(r,z,t) = -\frac{Ne\delta(r)}{2\pi r \Delta z} \exp\left[-(z_o/\Delta z)^2\right]$, one finds

$$E_z(r,z,t) = -E_o \sum_{m=0}^{\infty} \frac{f_m(r)}{\alpha_m} e^{-(\omega_m \Delta z/2v)^2} e^{-i\omega_m z_o/v}. \tag{14}$$

In Eqs. 13 and 14, $E_o = -Ne/4\pi\varepsilon_o a^2$ is the Coulomb field of the bunch at the edge of the hole, and causality dictates that the results are valid only behind the bunch, i.e. for $z_o \le 0$; ahead of the bunch the fields are of course zero.

Eq. 7 has been evaluated for a waveguide with a = 0.128 cm, R = 1.0 cm, and κ= 10.0. A relative dielectric constant of κ = 10.0 is close to the value of 9.6 for alumina. It is assumed that κ is independent of frequency. The phase velocity of all the *TM* modes corresponds to the speed of an electron bunch with γ = 13, i.e. $0.99704c$. Fig. 2 shows the eigenmode frequencies for this choice of parameters. For this case, the first frequency interval $(\omega_2 - \omega_1)/2\pi$ = 5.32 GHz, while the asymptotic interval $\Delta\omega/2\pi$ is 5.71 GHz. It is thus seen that conditions can be found where the eigenmodes all have equal phase velocities with nearly equal eigenfrequency spacings. The maximum deviation in frequency interval for the example shown in Fig. 2 is 6.8%, about double the value found for planar geometry [6].

III. Power output and field structure

The theoretical results of Section II were evaluated numerically for comparison with wake-field experiments conducted at Argonne National Laboratory [8]. Good agreement was obtained for the wake field structure, intensity and mode frequencies. In this case only the first few modes make significant contributions, as also noted by the Argonne group.

The detailed computations presented in this section are mostly for a Gaussian bunch of 1.0 mm length, but other bunch sizes are also taken for evaluations of the mode spectrum and energy loss. The wake field structure is examined for a total charge of 10 nC, although the results can be scaled in direct proportion to the total charge (so long as the bunch energy loss is not so great as to significantly reduce the bunch velocity). It is seen from Fig. 2 that, for this example, consideration of only the first few modes would give an incomplete picture of the wake field structure. Therefore, the wakefield is computed here by including modes up to $m = 50$ in the sum in Eq. 14, even though modes with the higher indices will make smaller contributions. For Q = 10 nC, the Coulomb field $E_o = 54.93$ MV/m. The computed spontaneous wake field pattern of a single bunch is shown in Fig. 3 for $0 \leq z_o \leq 30$ cm, i.e. at the instant that the bunch has traveled 30 cm into the waveguide. The wake field peaks are seen generally to alternate in sign; to each be relatively concentrated in z_o; and to have a period of 10.5 cm, corresponding to the vacuum wavelength at 2.856 GHz, i.e. half the asymptotic frequency interval $\Delta\omega/2\pi$. The peak values of E_z for the first wake at the bunch and at 5.2 cm behind the bunch are +20.51 and -19.40 MV/m, and later wakes develop secondary oscillations and are somewhat smaller. The waveguide length chosen is to allow a moderate 20% energy loss from the bunch, as will be discussed below. The radial distribution of axial electric field at different axial locations within the first half wake period is shown in Fig. 4. This figure shows that when the electron bunch passes through the waveguide, the emitted radiation

travels in a pulse moving at an angle with the waveguide axis until it reflects from the wall and heads back to the axis, forming a radiation cone reminiscent of a Cerenkov cone in free space. This reflection of the pulse from the wall back to the axis repeats periodically, and is responsible for the periodic sharp peaks in axial wake field shown in Fig. 3.

Fig. 5 shows the instantaneous (time-dependent) power structure, computed as

$$P = 2\pi \int_0^R dr r \left(\sum_m \vec{E}_m \right) \times \left(\sum_n \vec{H}_n \right) \cdot \hat{e}_z \ . \tag{15}$$

It is noted that terms with $m \neq n$ contribute to the instantaneous power and are responsible for the sharp spikes in Fig. 5. In the time-average power only terms with $m = n$ contribute. For this example, the peak power is 3.3 MW and the average power is 1.23 MW. Fig. 5a shows the full instantaneous power pulse, which occupies a time duration of 1 nsec. Fig. 5b shows an expanded plot of the sharp power spike near the center of the pulse, indicating the 3.3 MW peak with a width of 3 psec. Such unusual high-power psec pulses could find application in time-dependent spectroscopy or remote sensing.

The mode spectrum of the radiation is sensitive to the bunch length and profile. Shown in Fig. 6 is the wake field mode spectrum for a Gaussian bunch with a total charge -Ne = Q = -10 nC, for several bunch lengths Δz = 1, 2, and 3 mm. If the bunch length is increased the mode spectrum narrows, with diminished amplitudes for the higher frequency modes. Also, the narrower the bandwidth, the less dielectric dispersion (neglected here) will matter. The strong dependence of the width of the mode spectrum on bunch length could be the basis for a passive, non-intercepting diagnostic tool for monitoring bunch size for relativistic electron beams. Profiles with non-Gaussian shapes will have different mode spectra.

Now we turn to considerations of energy loss by the bunch. The rate of energy accumulation with distance in wake fields behind the bunch dW/dz is given by integrating the field energy density over the waveguide cross-section, thus leading to the following relation.

$$\frac{dW}{dz} = \frac{1}{4}\sum_{m=0}^{\infty}\int_0^{2\pi} d\theta \int_0^R rdr\left\{\varepsilon(r)\left[E_{r,m}^2 + E_{z,m}^2\right] + \mu_o H_{\theta,m}^2\right\}$$

$$= \frac{\varepsilon_o E_o^2 \pi R^2}{2}\sum_{m=0}^{\infty}\frac{h^2(\xi_m)}{\alpha_m^2}\left\{\frac{1}{R^2}\int_0^a I_0^2(k_{1m}r)rdr + \left(1+\beta^2\right)\gamma^2\frac{1}{R^2}\int_0^a I_1^2(k_{1m}r)rdr\right. \tag{16}$$

$$\left. + \kappa\left(\frac{I_0(k_{1m}a)}{P_0(k_{2m},R,a)}\right)^2\left[\frac{1}{R^2}\int_a^R P_0^2(k_{2m},R,r)rdr + \left(1+\kappa\beta^2\right)\frac{\gamma_k^2}{R^2}\int_a^R P_0^2(k_{2m},R,r)rdr\right]\right\}$$

The source current and charge distributions in Eq. 8 are assumed to remain constant during the interaction. If not, the individual mode amplitudes must be adjusted iteratively; this amounts to introduction of a z-dependent structure factor $h(\xi_m)$ in equations such as Eqs. 13 and 14. For the rectangular bunch, the structure factor $h(\xi_m) = (\sin\xi_m/\xi_m)^2$; and for the Gaussian bunch, $h(\xi_m) = \exp(-\xi_m^2)$, with $\xi_m = \omega_m \Delta z/2v$. For the parameters chosen and Q = 10 nC, Eq. 16 gives dW/dz = 4.01 x 10^{-2} J/m. Equating dW/dz to the energy loss rate $Q E_{drag}$ gives E_{drag} = 4.01 MV/m for a single bunch. This drag field will slow down the 6 MeV bunch to 4.80 MeV within 30 cm. For this example the efficiency for transfer of bunch kinetic energy into radiation energy is seen to be 20%. If the waveguide were to extend to 100 cm in length, this drag field would transfer 4 MeV of beam energy into wake field radiation, giving an efficiency of 67%. Larger energy loss by the bunch will result in reduction in the phase velocities of the wake field modes that are excited, with a corresponding change in the wake field pattern.

Measurement of the energy loss of a bunch traversing such a dielectric waveguide can also be used as a bunch length diagnostic, if the total bunch charge is known. This is illustrated in Fig. 7, which for a 10 nC Gaussian bunch shows the energy loss in traversing a 30 cm length of dielectric waveguide as a function of the bunch width Δz. It is seen that energy loss is a strongly decreasing function of increasing bunch length. This diagnostic method could be more easily implemented than the measurement of radiation spectrum, since the latter requires careful calibration of the detectors over a wide frequency range, while the former requires knowledge of only the bunch energy before and after traversing the dielectric waveguide. Of course, the spectrum can in principal be inverted to give the actual axial bunch profile, rather than only the effective width.

IV. An experimental test of certain features of this theory

A preliminary experiment was carried out to excite Cerenkov radiation in a cylindrical tube made of alumina, using an unbunched beam. The schematic of the experiment is shown in Fig. 8. The alumina tube has outer diameter 32 mm and fits into a copper pipe having an inner diameter of 33 mm; the axial hole through the alumina cylinder is 9 mm in diameter. The alumina cylinder is 110 cm long, and the electron beam is passed along a length of 85 cm before it is deflected to the wall by distorting the guide magnetic field using an iron "beam stop." An otherwise uniform guide magnetic field of approximately 0.9 T is provided for electron beam guiding and focusing. The electron beam has a diameter of about 3 mm and carries a current of about 100 A. The beam is extracted from a cold-cathode diode made of graphite, which field-emits when a 600 kV negative pulse is applied to the cathode. Only a small portion of the emitted current is passed through an aperture in the anode, a procedure which has been shown to improve the beam quality [9]. The diode is attached to a pulse-line accelerator, which applies a 150

nsec pulse of high voltage to the cathode. A pressure below 10^{-6} Torr is obtained in the diode and in the hole through which the beam propagates. Radiation exits the waveguide into air through a plexiglas window which is cemented onto the end of the alumina cylinder.

Radiation was initially picked up by several detectors connected to sections of waveguide used as high-pass filters. The strongest signals were obtained at S-band, for which the TM_{01} mode should match the electron speed ($0.97c$) at 2.9 GHz. From the geometry of the system and the calibration of the detectors, it is estimated that MW levels of radiation were observed for pulses lasting <100 nsec. However, it was found that the radiated power could be propagated in X-band and K-band waveguides as well. This suggested that higher modes were being excited, so a quasi-optical grating spectrometer was installed to study the spectrum of the radiation at wavelengths shorter than 12 mm [10]. An example of this spectrum is shown in Fig. 9. The horizontal axis is labeled in frequency units, with the frequencies of the peaks indicated; the spectrometer was calibrated against a 24 GHz source. The data points reflect averages with a standard deviation of roughly 30%. In addition to the peak frequencies indicated on this figure, another peak of radiation was observed at 39 GHz, but very little beyond 40 GHz. The spacing of the modes is seen to be about 4 GHz.

In Table I we compare the observed peak frequencies radiated versus the mode frequencies predicted from the dispersion relation, Eq. 7 of Section II, using a dielectric coefficient of 10 for alumina. The frequency spacing predicted was about 4.3 GHz, and the mode number is also indicated. The theory appears to be in relatively good agreement with the experimental results for the mode frequencies.

It is not unreasonable to ask why this system should radiate high power at the discrete frequencies as predicted by theory, since the beam is initially unbunched whereas the theory is appropriate to either one bunch or to a sequence of bunches. We point out that the observed level of power radiated cannot be explained without the presence of considerable bunching. Evidently a linear beam Cerenkov instability is present that leads to rapid bunching. While the bunching is probably not nearly so distinct as used in the theory, it is apparently enough to excite a mode spectrum up to $m \sim 9$. Thus it seems reasonable to compare the results of this experiment with the theory of Section II; but we emphasize that this experiment does not check other features of this theory, such as the wakefield or the time-structure of the emitted power.

V. Conclusions

By exciting a dielectric-loaded waveguide system with short bunches of electrons, theory predicts that high power microwave pulses of Cerenkov radiation are emitted with picosecond-scale time variations. This occurs because the short bunches excite a highly localized wake field which trails the electron bunch in the waveguide. The wake field is made possible by the coherent superposition of many discrete *TM* waveguide modes. We have studied the example of 6 MeV, 10 nC bunch, which can be obtained from a conventional rf gun driven by a high power pulsed klystron at 2.856 GHz. The example showed that 20% of the kinetic energy in the pulse can be converted into radiation, with up to 3.3 MW peak power having width of a few psec. This is achieved using a short section of waveguide, and only a single bunch is analyzed. When more than one bunch is present in the waveguide, much higher radiation power may be reached. To our knowledge, this is the first time that this approach to the generation of psec MW-level microwave power has been discussed. This radiation could find applications in material studies or remote

REFERENCES

1. J.E. Walsh, T.C. Marshall, and S.P. Schlesinger, "Generation of coherent Cerenkov radiation with an intense relativistic electron beam", Phys. Fluids. vol. 20, pp. 709-710, 1977.
2. J.E. Walsh and E. Fisch, "Radio-frequency-injector driven Cerenkov free electron laser", Nucl. Instrum. Methods A, vol. 318, pp. 772-774, 1992.
3. W. Main, R. Cherry, and E. Garate, "200 MW S-band dielectric Cerenkov maser oscillator", Appl. Phys. Lett., vol. 55, pp. 1498-1500, 1989.
4. J. Walsh, "Stimulated Cerenkov Radiation", Adv. Elect. and Electron Physics, C. Marton ed., vol. 58, pp. 271-310 (Academic Press, 1982).
5. T.B. Zhang, T.C. Marshall, M.A. LaPointe, J.L. Hirshfield, and Amiram Ron, "Microwave inverse Cerenkov accelerator", Phys. Rev. E, vol. 54, pp. 1918-1929, 1996.
6. T.B. Zhang, J.L. Hirshfield, T.C. Marshall, and B. Hafizi, "Stimulated dielectric wake-field accelerator", Phys. Rev. E, vol. 56(to be published), October 1997
7. M. Borland, private communication.
8. W. Gai, P. Schoessow, B. Cole, R. Konecny, J. Norem, J. Rosenzweig, and J. Simpson, "Experiment demonstration of wake-field effects in dielectric structures". Phys. Rev. Lett., vol. 61, pp. 2756-2758, 1988.
9. S.C. Chen and T.C. Marshall, "Parallel velocity spread induced in a relativistic electron beam by an undulator", IEEE J. Quantum Electronics vol. 21, pp. 924-930, 1985.
10. J.A. Pasour and S.P. Schlesinger, "Multichannel grating spectrometer for millimeter waves", Rev. Sci. Instrum. vol. 48, pp. 1355-1356, 1977.

Table I. Comparison of theoretical and experimental mode frequencies

Mode number	f_6	f_7	f_8	f_9
Theoretical (GHz)	23.96	28.32	32.68	37.06
Experimental (GHz)	23	27	31	35

FIGURE CAPTIONS

Fig. 1. Schematic for a Cerenkov wakefield wide band radiation system. The dielectric-lined waveguide is used for wakefield generation. The radii of waveguide and empty hole are R and a respectively.

Fig. 2. Wakefield mode frequencies.

Fig. 3. Wakefield radiation from a 10 nC, 6 MeV, 1 mm long Gaussian bunch after it has traveled 30 cm left to right in the cylindrical waveguide.

Fig. 4. The radial distribution of axial electric field at several axial locations of the first half wake period.

Fig. 5. (a) Wakefield power distribution from a 10 nC, 6 MeV, 1 mm long Gaussian bunch after it has traveled 30 cm left to right in the cylindrical waveguide; (b) An extended plot of the sharp power spike near the center of the pulse.

Fig. 6. Wakefield power spectrum for variable bunch lengths.

Fig. 7. The energy loss by Cerenkov radiation as a function of bunch length for a 10 nC Gaussian bunch traversing a 30 cm long waveguide.

Fig. 8. The schematic of the experiment demonstrating the wakefield generation in the alumina-loaded cylindrical waveguide. The unbunched beam is used for this experiment.

Fig. 9. Power spectrum of the wakefield emitted from the experiment shown in Fig. 8.

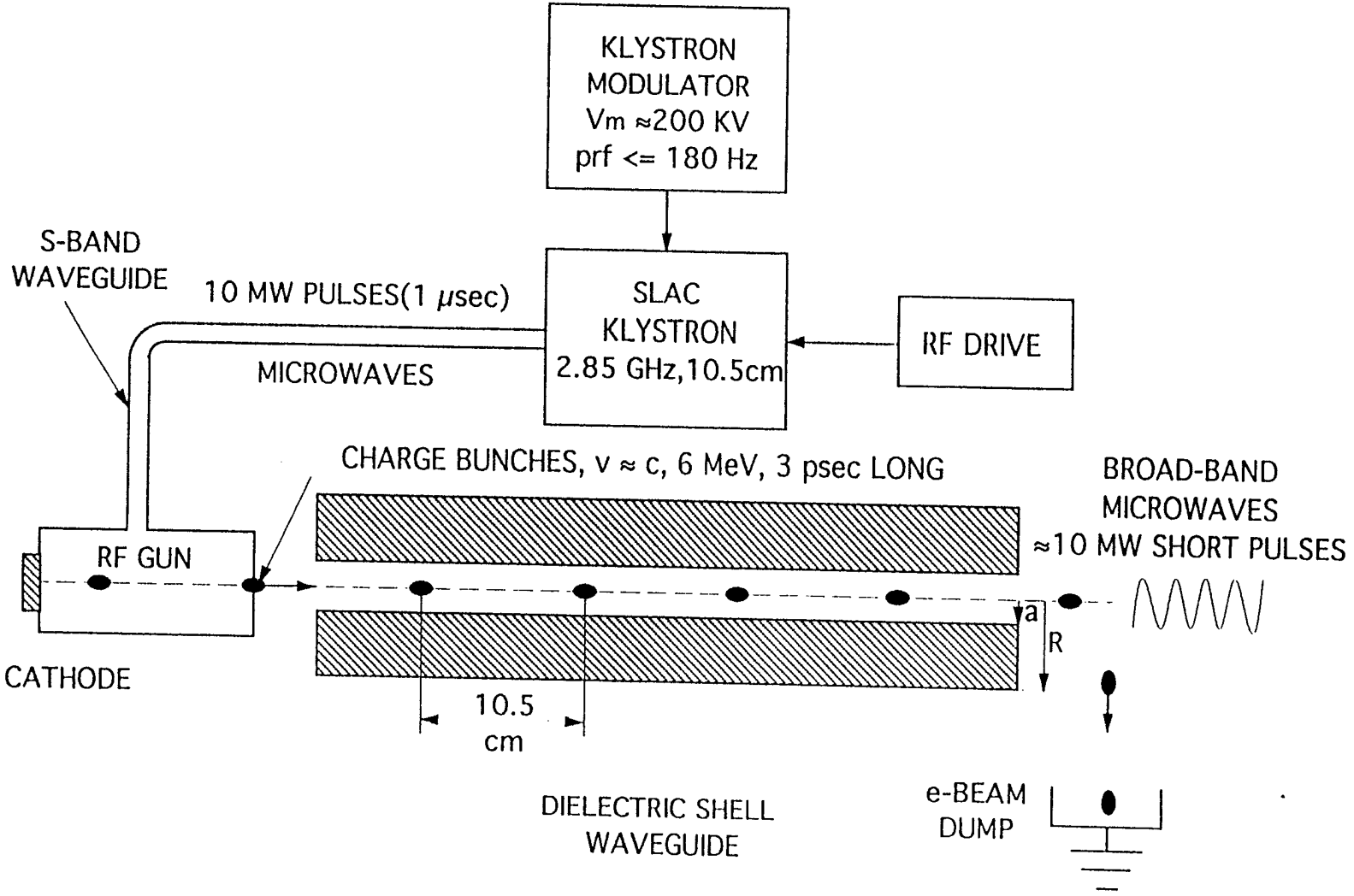
KLYSTRON
MODULATOR
Vm ≈200 KV
prf <= 180 Hz
S-BAND
WAVEGUIDE
10 MW PULSES(1 μsec)
MICROWAVES
SLAC
KLYSTRON
2.85 GHz,10.5cm
RF DRIVE
CHARGE BUNCHES, v ≈ c, 6 MeV, 3 psec LONG
BROAD-BAND
MICROWAVES
≈10 MW SHORT PULSES
RF GUN
a
R
CATHODE
10.5
cm
DIELECTRIC SHELL
WAVEGUIDE
e-BEAM
DUMP

Fig.1

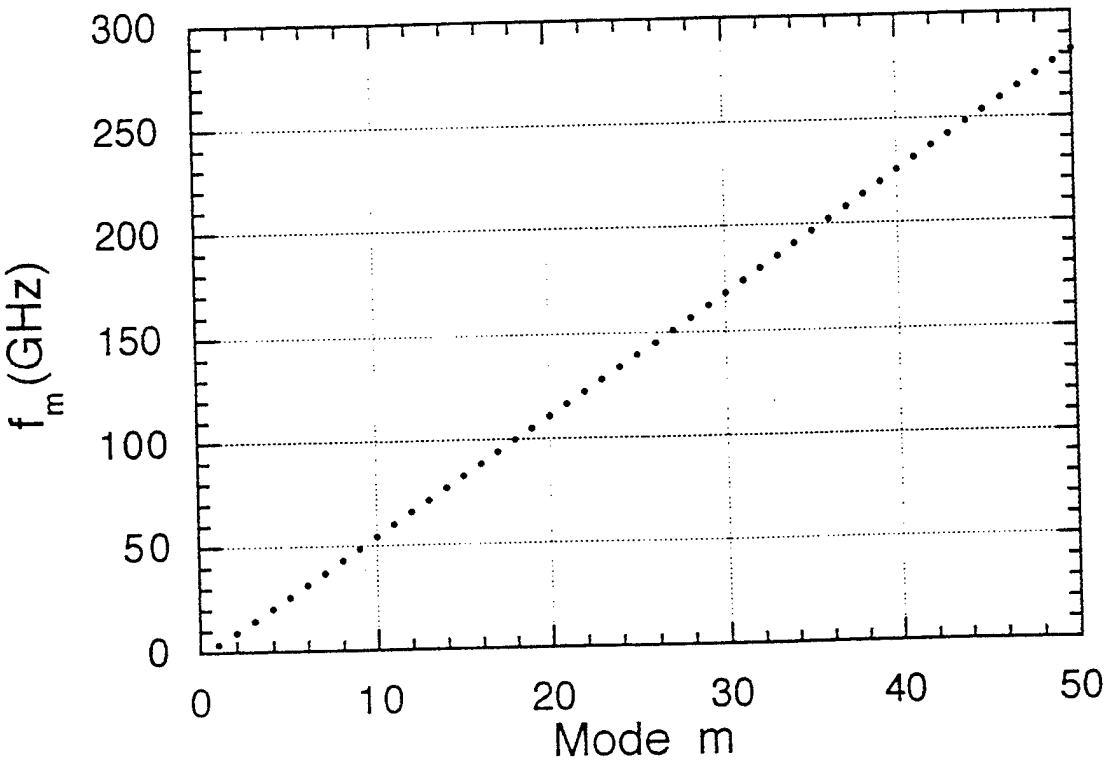

Fig. 2

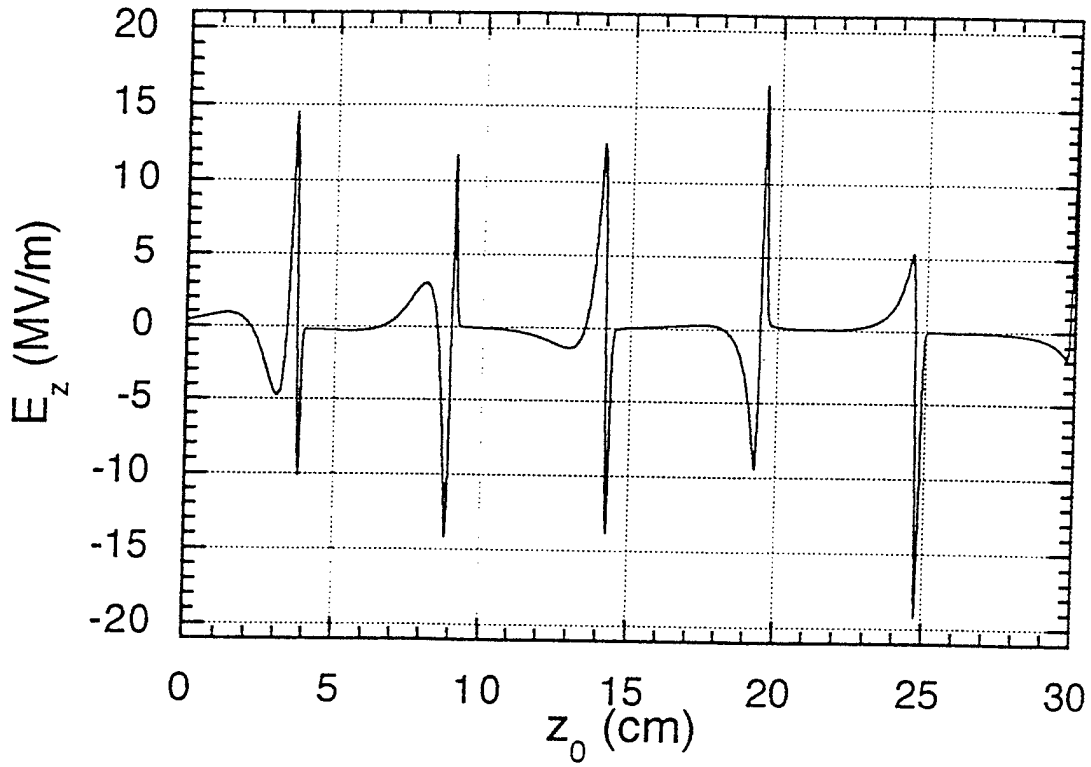

Fig. 3

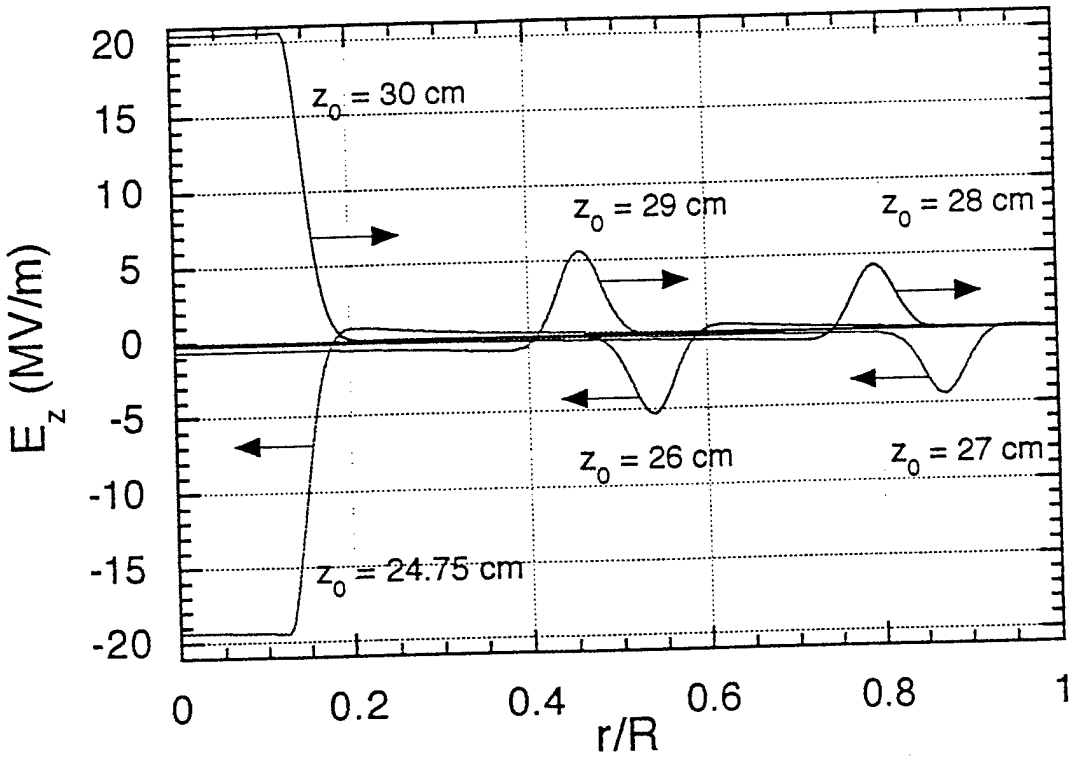
20
15
10
5
0
-5
-10
-15
-20
E_z (MV/m)
0
0.2
0.4
0.6
0.8
1
r/R
z_0 = 30 cm
z_0 = 29 cm
z_0 = 28 cm
z_0 = 26 cm
z_0 = 27 cm
z_0 = 24.75 cm

Fig.4

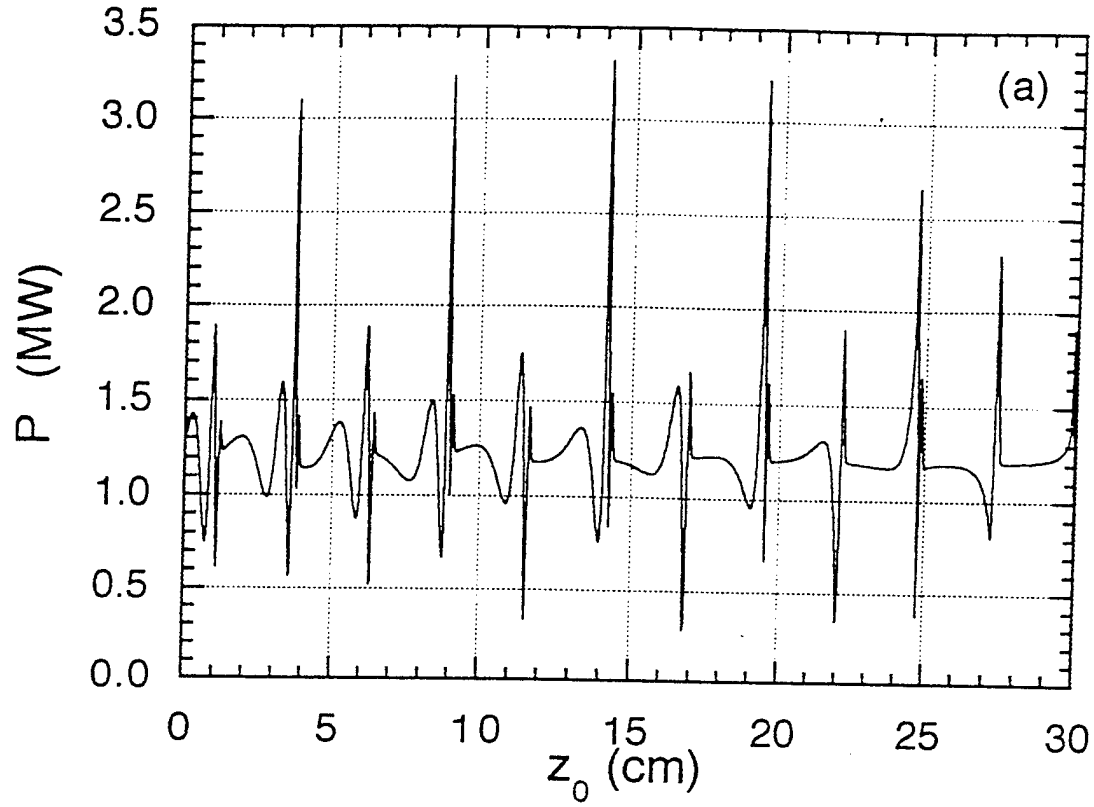
(a)
P (MW)
3.5
3.0
2.5
2.0
1.5
1.0
0.5
0.0
0
5
10
15
20
25
30
z_0 (cm)

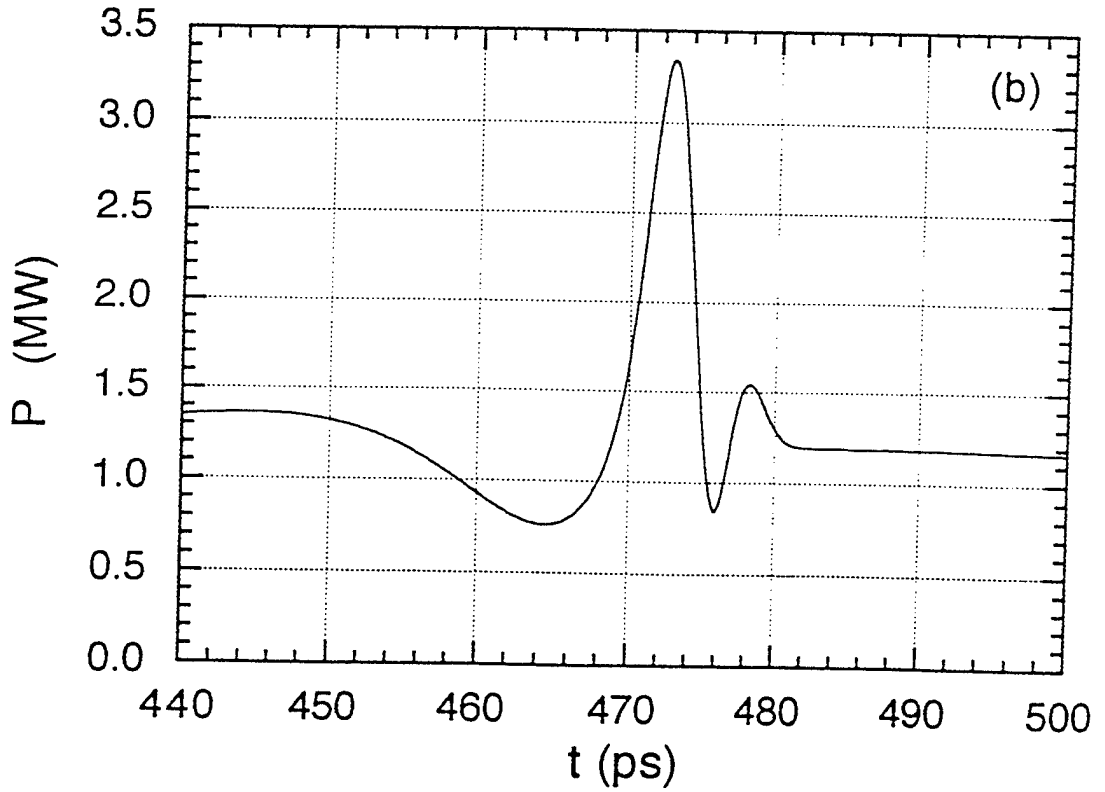
(b)
P (MW)
3.5
3.0
2.5
2.0
1.5
1.0
0.5
0.0
440
450
460
470
480
490
500
t (ps)

Fig. 5

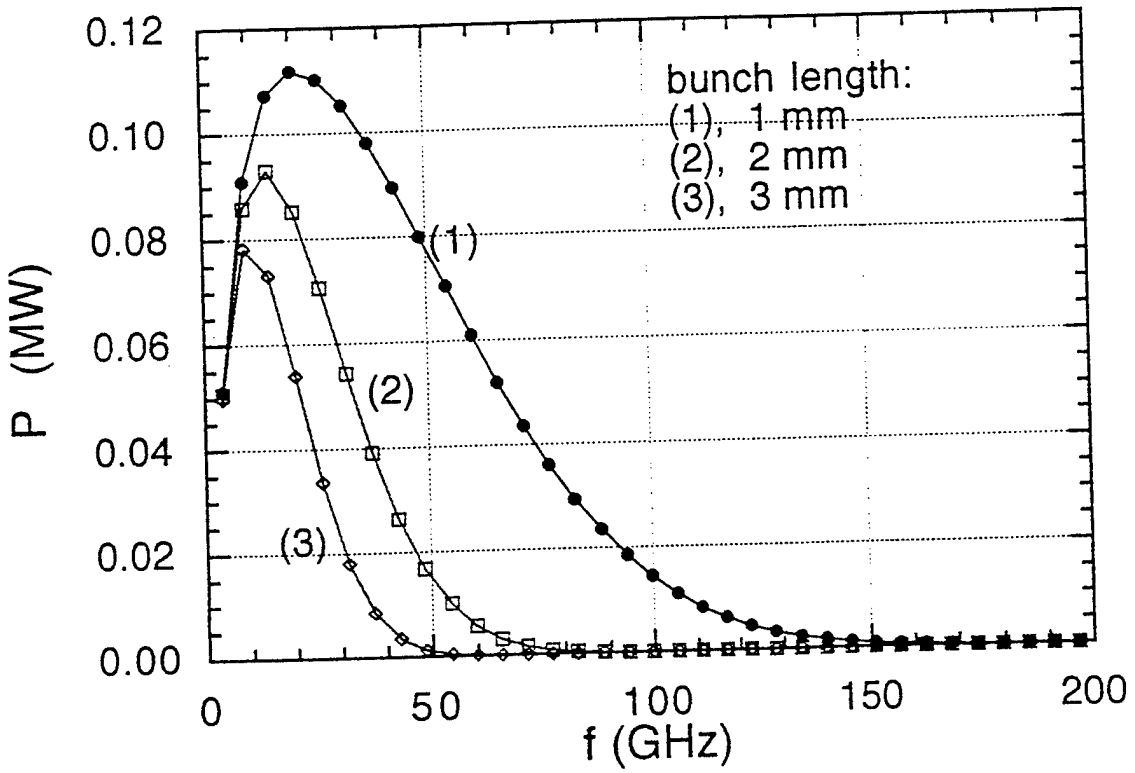
0.12
0.10
0.08
0.06
0.04
0.02
0.00
P (MW)
0
50
100
150
200
f (GHz)
bunch length:
(1), 1 mm
(2), 2 mm
(3), 3 mm
(1)
(2)
(3)

Fig.6

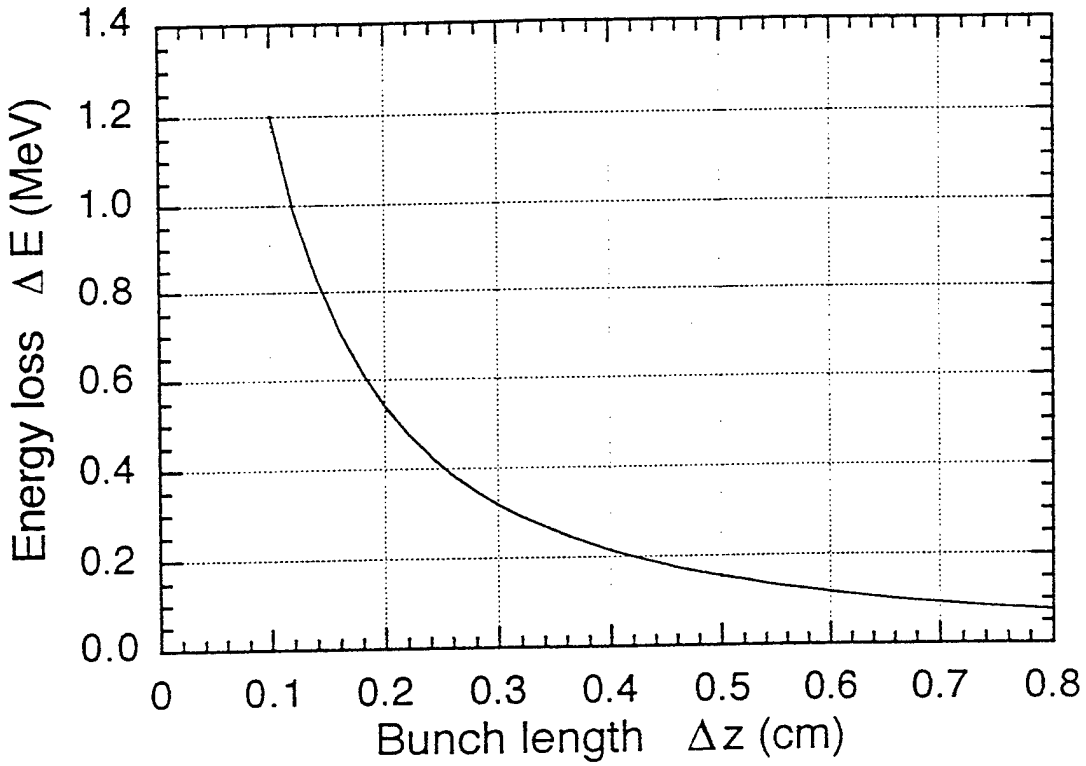
1.4
1.2
1.0
0.8
0.6
0.4
0.2
0.0
Energy loss ΔE (MeV)
0
0.1
0.2
0.3
0.4
0.5
0.6
0.7
0.8
Bunch length Δz (cm)

Fig. 7

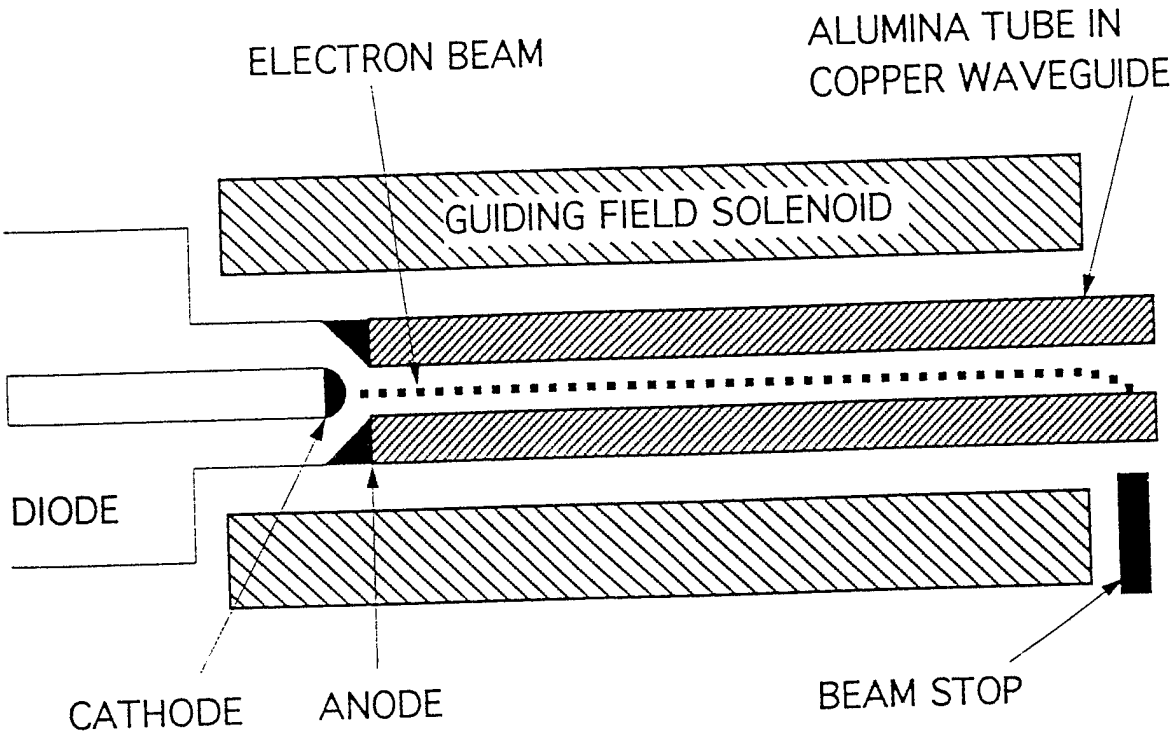
ELECTRON BEAM
ALUMINA TUBE IN
COPPER WAVEGUIDE
GUIDING FIELD SOLENOID
DIODE
CATHODE
ANODE
BEAM STOP

Fig 8

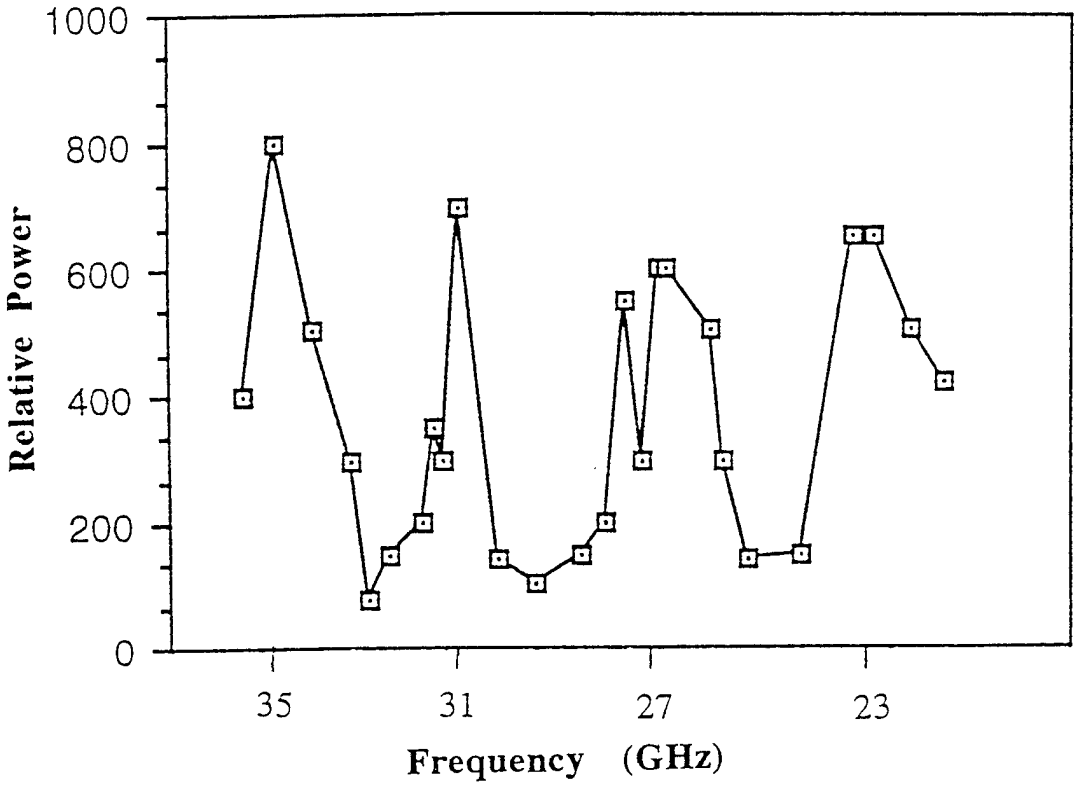
1000
800
600
400
200
0
Relative Power
35
31
27
23
Frequency (GHz)

Fig.9

III.

PHYSICAL REVIEW E VOLUME 56, NUMBER 2 AUGUST 1997

Harmonic millimeter radiation from a microwave free-electron-laser amplifier

Y-H. Liu and T. C. Marshall
Department of Applied Physics, Columbia University, New York, New York 10027
(Received 20 January 1997)

Using a free-electron laser (FEL) configured as a traveling-wave amplifier, we have caused the bunching produced by the amplification of a coherent microwave source to drive appreciable power at the harmonics. A 10-kW 24-GHz microwave input signal grows to the ~200 kW level using the lower frequency unstable root of the waveguide FEL dispersion relation. The FEL operates in the TE11 mode, using a helical undulator (1.85-cm period) and a 3-mm-diam 600-kV electron beam contained in an 8.7-mm-i.d. cylindrical waveguide. The harmonic currents set up by the microwave are found to cause growth of harmonic power under two conditions. First, if the design is such that the upper frequency root corresponds to the third harmonic, we see small amounts of third- and second-harmonic power, coherent with the source. Second, we have found kW emission of the seventh harmonic, most likely from the TE72 mode, which travels at the same speed as the 24-GHz wave. In order to excite the seventh-harmonic radiation, the electron beam must be displaced from the axis of the guide by ~2 mm. In both cases, no harmonic power is produced without gain at the fundamental. We present a one-dimensional theoretical model of the experiment, and use the numerical results to interpret our findings. The model predicts that if the microwave signal is strong enough to drive the FEL into saturation, the harmonic radiation should become powerful. [S1063-651X(97)14108-3]

PACS numbers: 41.60.Cr

INTRODUCTION

If an electron beam undergoing FEL (free-electron laser) interaction is bunched by a coherent source of power, then FEL harmonic radiation will grow from an initial condition that is very much above noise input. The radiation at the harmonics should be related in phase and frequency to the source, which bunches the electron beam. However, lacking some resonant or phase-matching process, typically harmonic radiation remains at a low level [1]. Appreciable harmonic power depends on gain at the FEL harmonic [2], or on some mechanism to couple energy from the lower frequency FEL wave into the harmonic. In this paper we study an example of each of these.

Recently, Pioveila *et al.* [3] studied a waveguide FEL where the beam is bunched by a growing wave at the low frequency beam-wave intersection, prompting growth at a harmonically related high frequency upper intersection [see Eq. (1) below]; a similar idea was described by Sternbach and Ghalila [4]. In the waveguide FEL, there are two unstable roots of the dispersion relation that represent. in the work we describe in this paper, growing TE11 waves at 24 and ~72 GHz (third harmonic); the frequencies are obtained approximately by calculating the intersections between the beam wave dispersion and the electromagnetic wave dispersion curves in a waveguide, neglecting the Raman space charge effect:

$$\omega_{1,2}=\frac{\omega_s}{1-\beta}\left[1\mp\beta_z\sqrt{1-X}\right]. \tag{1}$$

where $\omega_s=c\beta k_w/(1-\beta)$ and $k_w=2\pi/l_w$. X involves the cutoff frequency of the waveguide. $X=[(1.84/2\pi R_g)l_w/\beta\gamma_1]^2$. Here, $\beta c=v_z$ the axial electron velocity, γ_1 is the corresponding relativistic factor, l_w is the undulator period, R_g is the cylindrical waveguide radius, and c is the speed of light. Thus one might generate frequency and phase stable millimeter power in a FEL amplifier using a microwave source for bunching; and because the high frequency harmonic wave in the FEL is also growing, the power output in principle can be high. We have reported already on an experiment that studies such harmonic radiation from a FEL—configured as a traveling-wave amplifier—using a magnetron source to drive the low frequency FEL mode [5].

In this paper, we give further data and interpretation regarding the experimental properties of this interaction. Also, our recent observation [6] of appreciable *seventh*-harmonic power is a potentially significant development, and involves a mechanism that is different [7] from that described above; we shall present experimental results and interpretation of this effect as well. In the following, we present a theory and a numerical simulation of the experiments that makes use of the FEL equations using two waves, harmonically related in frequency but traveling at different speeds in a waveguide.

EXPERIMENT

Figure 1 shows a schematic of the FEL apparatus, which is driven by a pulseline generator [8]. This pulseline produces a 150-nsec, nearly flat voltage pulse (400–600 kV).

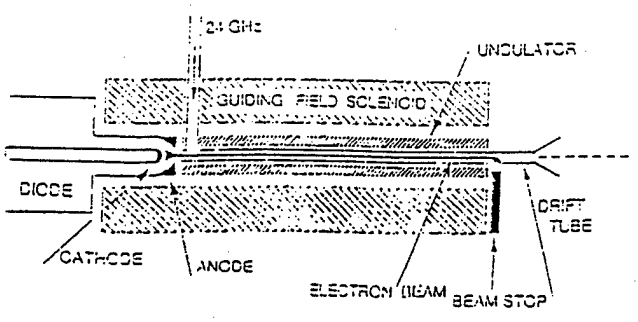

FIG. 1. Schematic: a pulseline source provides a negative 150-nsec pulse to a graphite diode that "apertures" the electron beam.

TABLE I. Parameters of the FEL.

	Col. 1	Col. 2
Electron energy	600 kV	
Low frequency FEL mode	24 GHz	
High frequency FEL mode	72 GHz	
Undulator period	2.5 cm	1.85 cm
a_w, effective undulator parameter	0.2	
Guide field	0 G	8800 G
TE11 cutoff frequency	18.4 GHz	20.7 GHz
Electron beam current	~100 A	
Electron beam diam	~3 mm	

which is applied to a cold graphite cathode in a field-immersed vacuum diode. The solenoidal field is primarily for beam transport, but it also slightly enhances the spiraling motion of the electrons moving through the undulator (quiver velocity $\sim 0.1c$). The electron current emitted from the cathode is "apertured" by a 3-mm-diam hole in a graphite anode to improve the beam quality: the beam carries about 100 A. Table I lists parameters of the device appropriate to the experiment, which is conducted in the "Raman" regime (column 2), whereas the first column refers to equivalent parameters for the "Compton" theory. A 24-GHz 10-kW signal obtained from a magnetron is launched in the TE11 mode inside a cylindrical stainless steel waveguide, enclosed by a helical undulator. A relatively small value of undulator field (~250 G) is chosen so that the system behaves like a traveling-wave amplifier with a gain <50, in which case oscillation is avoided; also, numerical study of the electron motion has shown that a low undulator field will give stable well-behaved electron orbits in the combined undulator and guide fields. The propagation and alignment of the electron beam through the waveguide were studied by taking a series of "witness plates." (The latter determines the beam location via a damage pattern on a piece of thermal-sensitive paper.) The diameter of the waveguide and undulator period are chosen so that there is exponential gain of the 24-GHz wave and one of the harmonics at an electron beam energy of 600 kV: a single frequency code [9] that includes the one-dimensional (1D) motion and the 2D wave equations in the cylindrical waveguide was used for this design. Figure 2 shows the computed gain [9] of the device for beam energies of 600 and 400 kV, taking the fundamental and harmonic waves to be in the TE11 mode.

Using a grating spectrometer adapted for millimeter-wave studies [10], we have found 24-GHz power gain ~20 (well below saturation), and the observation of the first three harmonics (~100 W, peak) has been reported [5]. No harmonic power is obtained unless there is appreciable gain for the 24-GHz wave (compare corresponding traces, Fig. 3). The third-harmonic power output was found to be greater than the second, and both are much greater than the fourth (Fig. 4) or higher harmonics. If the interaction were nonresonant, then the power of the harmonics should fall off very rapidly [1] with increasing harmonic number. The power gain at 72 and 48 GHz for the operating condition of beam voltage of 600 kV should be about 10, according to Fig. 2; this figure shows the gain maxima that result from the two intersections described by Eq. (1). Figure 3 shows the result (lower trace)

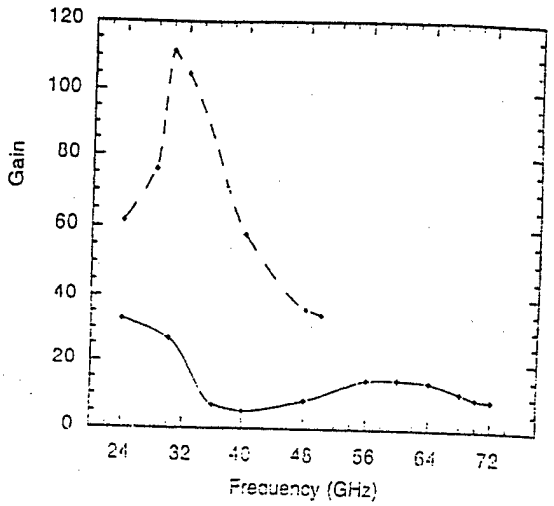

FIG. 2. Computed FEL gain vs frequency, for parameters of Table I, column 2, for beam energy of 600 kV (solid line) and 400 kV (dashed line).

of mixing the 72-GHz FEL third-harmonic signal with the frequency tripled magnetron signal, demonstrating a fixed frequency relationship between the FEL third-harmonic power pulse and the lower frequency magnetron power that drives the FEL bunching.

We have also observed the emission of appreciable seventh-harmonic power, 168 GHz (spectrum, Fig. 4), obtained only when we have appreciable gain for the 24-GHz FEL wave and when there was a misalignment of our system in which the electron beam was moved about 2 mm off the waveguide axis. The seventh-harmonic signal level is ~1 kW or more, whereas the 24-GHz signal is amplified to ~200 kW, much less than saturation. The seventh harmonic is not a "resonant FEL interaction" and its appearance should depend on two special conditions. The first is that the

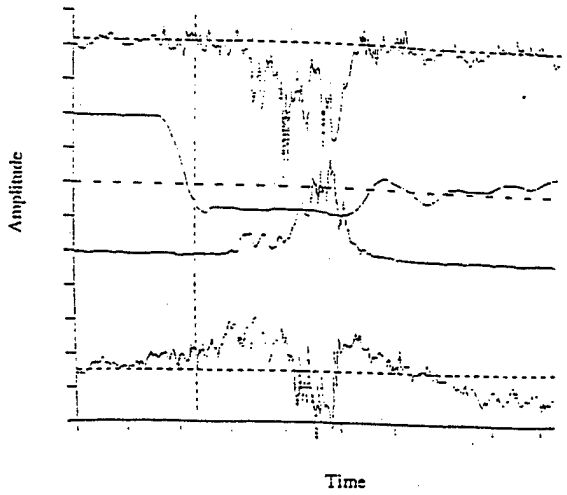

FIG. 3. From below: beat signal envelope of FEL third harmonic mixed with magnetron tripled frequency; 24-GHz amplified signal; diode voltage of accelerator (~600 kV); 72 GHz detector signal. Horizontal scale: 50 nsec/div; diode voltage vertical scale: 200 kV/div.

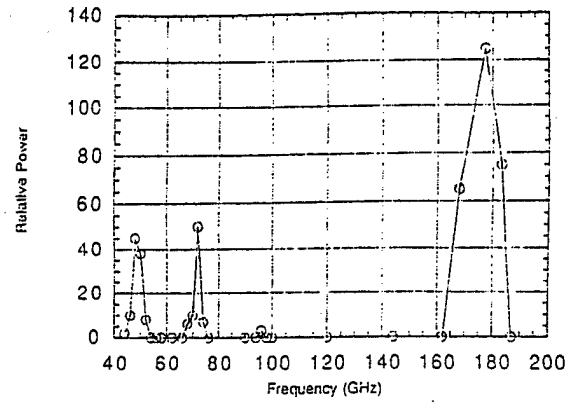

FIG. 4. Power spectrum scan, covering harmonics 2–8: beam is off axis for harmonics >5 (signals for the seventh harmonic and harmonics >5 are zero for on-axis beam). Data points represent average of several shots, recording peak power.

temporal and spatial spectrum of the seventh-harmonic electromagnetic wave must move at very nearly the same wave velocity as the temporal and spatial spectrum of its electron current source, the latter being set up by the seventh temporal harmonic of the bunching caused by the amplified TE11 24-GHz wave. The EM wave in question that satisfies this constraint is the TE72 mode of the cylindrical waveguide [7], since this wave has the same wave refractive index as the TE11 wave at 24 GHz. Also, this mode has zero field on axis, and therefore the electron beam must be moved off axis to overlap one of the electric field maxima of the TE72 wave. We have observed the seventh-harmonic signal in this device for an electron beam energy of 600 kV and as low as 400 kV (Fig. 5), since there is gain at 24 GHz at the lower energy (see Fig. 2).

In contrast to the "second-order" FEL resonant wave interaction (which commences from zero source current and field, apart from noise, but grows exponentially), the harmonic conversion is a "first-order" process [11], in which the beam is already prepared so that its equilibrium current carries spatiotemporal modulation at the harmonic (this modulation is set up by the FEL resonant interaction at 24 GHz). Thus there is no need for a "linearized dispersion relation" for the first-order conversion. What must happen, however, is that the wave that feeds on the seventh-harmonic currents in the beam must travel at the same speed as these currents if there is to be efficient conversion. The FEL interaction, which generates a wide spectrum of harmonics as the beam becomes progressively more bunched, is the free energy source for the seventh harmonic.

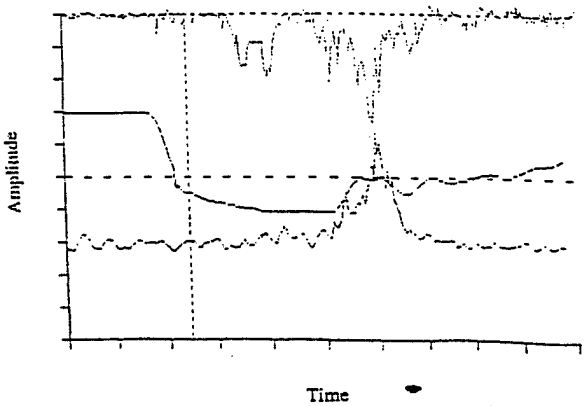

FIG. 5. 24-GHz amplified power (below) and 168-GHz converted power (above), obtained when the diode voltage (middle) is only about 400 kV; similar result can be obtained at 600 kV as well. Same scale axes as Fig. 3.

THEORY

To study the coupling between the harmonically related waves, we solve numerically the set of FEL equations with slippage for the electron dynamics and two interacting waves [5]. For simplicity, we disregard the space-charge (Raman effect), which will decrease the gain and require a shorter undulator period to provide the same frequencies as used in this calculation. The parameters of the calculation are given in Table I, column 1. The low-frequency (24 GHz) TE11 FEL mode has group velocity $\sim c/2$, as does the seventh-harmonic TE72 wave: the second- and third-harmonic TE11 FEL wave group velocities are higher than the electron speed ($\sim 0.88c$).

We first define the variables x and y as

$$x = A\left[t - \frac{z}{v_{g2}}\right], \quad y = A\left[\frac{z}{v_{\parallel}} - t\right],$$

where $A = [1_w(1/v_{\parallel} - 1/v_{g2})]^{-1}$ and v_{g1}, v_{g2} are the group velocities of ω_1 and ω_2, $v_{\parallel}$ is the electron axial speed, and z, t are the axis and time variables. Defining a_1 and a_2 ($a_1 = a_{s1}e^{-i\phi_1}$) as the normalized vector potentials of waves 1 and 2, which have axial wave numbers k_1 and k_2 in the waveguide, respectively, and a_w the undulator potential $eB_w l_w/2\pi mc^2$, where B_w is the undulator field, the electron and wave equations for the jth electron are

$$\frac{\partial \theta_{2j}}{\partial x} = l_w \bar{k}_{w2}\left(1 - \frac{\bar{\gamma}_{r2}^2}{\gamma_j^2}\right), \tag{2}$$

$$\frac{\partial \gamma_j}{\partial x} = -l_w \frac{a_w}{\gamma_j v_{\parallel j}}\left[\omega_1 a_{s1}\sin(\alpha\theta_{2j} + \phi_{1j}) + \omega_2 a_{s2}\sin(\theta_{2j} + \phi_{2j})\right], \tag{3}$$

$$\left\{\frac{\partial}{\partial y} + \left(\frac{1/v_{g1} - 1/v_{g2}}{1/v_{\parallel} - 1/v_{g1}}\right)\frac{\partial}{\partial x}\right\} a_1 = \frac{i}{A(1/v_{\parallel} - 1/v_{g1})}\frac{\omega_p^2 a_w}{2c^2 k_1}\left\langle\frac{e^{-i\alpha\theta_2}}{\gamma}\right\rangle, \tag{4}$$

$$\frac{\partial a_2}{\partial y} = i l_w \frac{\omega_p^2 a_w}{2c^2 k_2}\left\langle\frac{e^{-i\theta_2}}{\gamma}\right\rangle. \tag{5}$$

These equations also involve the following quantities: ω_p, the beam plasma frequency; α, the harmonic number; $\theta_2 = k_w z + k_2 z - \omega_2 t$; $\phi_{1,2}$, the optical phase; and

$$\bar{k}_{w2} \equiv k_w + k_2 - \omega_2/c, \quad \bar{\gamma}_{r2}^2 \equiv k_2(1 + a_w^2)/2\bar{k}_{w2}.$$

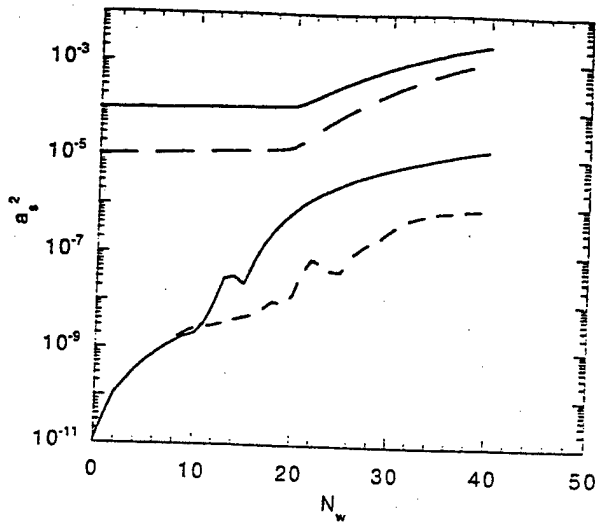

FIG. 6. 24-GHz FEL power growth (line pair above) and 168-GHz power converted (line pair below) in units of normalized wave vector potential squared, vs axial distance measured in undulator periods. There is a 1% mismatch of wave group velocity, and two cases are shown: for initial 24-GHz microwave power of 10 kW (broken lines) and 100 kW (solid lines).

In the simulation, the FEL behaves as a traveling-wave amplifier. The spatial distribution of simulation electrons has a rectangular profile, the electrons are taken to be monoenergetic, and at the undulator entrance $z=0$ they are uniformly distributed inside the beam length with 100 simulation electrons per undulator period. For each wavelength-size strip of particles, the relative phase location of the electrons with respect to the radiation field is uniformly distributed between $-\pi$ and π. For the output format of the computational results, the electron beam pulse and the radiation pulse (each taken to be flat-topped) are plotted as a function of the variables x and y, which imply two moving "windows," the former at v_{g2} and the latter at v_{g1}; both are scaled in units of the undulator period. The electron motion is parallel to the x axis while the ω_2 wave moves parallel to the y axis; the ω_1 wave moves along the characteristic

$$x-\left(\frac{1}{v_{g1}}-\frac{1}{v_{g2}}\right)\left(\frac{1}{v}-\frac{1}{v_{g1}}\right)^{-1}y=\text{const.}$$

The finite radial size of the electron beam is accounted for in the code using a multiplicative "filling factor" for the radiation current term on the right-hand sides of Eqs. (4) and (5). While this can be estimated from geometry, it is also a convenient parameter to adjust the gain of the 24-GHz wave so that it corresponds to our observations.

Figure 6 is an example we calculated that is relevant to the seventh-harmonic experiment. It shows the peak power growth along the undulator of the 24- and 168-GHz waves starting from an initial signal of 10 kW at 24 GHz in the right circular "rotating" mode; the two waves travel at nearly the same speed (the group velocity is about $0.5c$ in the waveguide). The figure shows that the conversion of microwave power to the seventh harmonic is ~7% when the signal reaches the end of our undulator, ~32 periods. This calculation (broken line pair) is for a wave speed mismatch

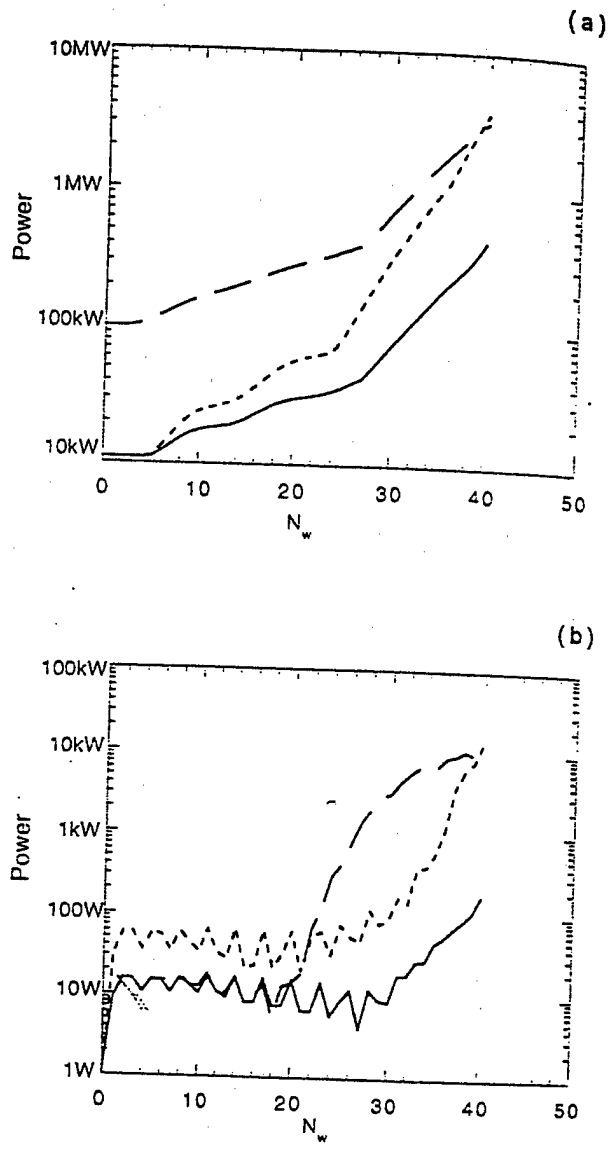

FIG. 7. Power growth of 24 (a), and 72 GHz (b) waves vs axial distance measured in undulator periods. The three examples are as follows. Solid line: initial microwave power 10 kW and gain of 40; dashed line: initial microwave power 100 kW and gain of 40; dotted line: initial microwave power 10 kW and gain of 400. The first case is that of the experiment where ~100 W at 72 GHz is produced; in the other examples, the 72-GHz power level is ~10 kW at 40 undulator periods. The gain of the 24 GHz wave is varied by changing the beam filling factor: 0.2 for low gain (experimental), and 0.35 for the higher gain example.

(between the 24- and the 168-GHz signals) of 1%, approximately what is expected from the theory [7]. However, if the FEL output is driven near saturation (~2 MW, solid line pair), the computation reveals that the seventh-harmonic power becomes nearly 30% of the microwave power. We point out that this is a 1D simulation and the overlap between the particles and the different radiation modes is being modeled with the same filling factor. Since a 3D simulation is really necessary to model the off-axis behavior of the beam and its overlap with the waveguide mode, the results of this calculation cannot be compared with the experiment quanti-

tatively, but may serve as an incentive for further study. Indeed, a 3D code [12] has been used recently to model the generation of the seventh-harmonic signal. Appreciable seventh-harmonic output (~2 kW) has been found [13] using the Raman version of this code with the electron beam located off axis; much smaller power (~200 W) was found when the beam was located on axis. These results, which are not much different from our experimental findings, will be presented in more detail elsewhere, as the optimum location of the electron beam for power conversion has yet to be found.

Figure 7 shows the increase of 24-GHz (power gain =40) and 72-GHz power, starting from 10 and 100 kW of the 24-GHz signal. The two waves travel, respectively, at a group velocity of $\sim c/2$, and $0.96c$. This is the "beam-on-axis" case, where the particles couple to the TE11 mode. The third-harmonic power reaches a level of 100 W and 10 kW, respectively. Another example is computed where the low frequency wave starts off at 10 kW, but experiences a power gain ~400. By comparing these examples, one finds that in order to get harmonic power of tens of kW it is necessary to have either a large input microwave power or a high-gain system: the requirement is that the device achieves a microwave power output near the saturation level so that the harmonics of the bunching are large [1]. The figure shows that the harmonic output is very sensitive to the output microwave power; we find that as much as 70 kW of third harmonic can be produced if the computation is carried further along to 50 undulator periods. The simulation, which compares with the experiment (solid line), shows the emission of only a small amount of power, as we have found. The harmonic power begins its rapid growth when the bunching produced by the microwaves develops a substantial harmonic component; until then (at $N_w<20$), the bunching harmonic and its wave amplitude remain small and "noisy" [1].

CONCLUSIONS

We believe the harmonic power observed in this experiment can be of use to create coherent, phase-referenced power in the millimeter spectrum for applications such as radar and accelerator physics. The higher frequency waves are driven by the bunching set up by the microwave source, and we have shown in the example of the third harmonic that this signal has a fixed relationship to the lower frequency source. The third-harmonic radiation does not compete with the seventh for the free energy of the bunching, because the seventh harmonic does not occur when the electron beam is positioned on the axis. On the other hand, one can suppress the lower harmonics by making the FEL interaction resonant at *one* microwave frequency only [by arranging that the second term in the square brackets of Eq. (1) vanishes], together with positioning the electron beam *off*-axis to enhance the seventh-harmonic coupling. The latter approach may represent a very convenient way to generate appreciable 2-mm wavelength power, using a FEL operating at comparatively low beam energy driven by a powerful microwave source. In our experiment, due to low gain of the system (~13 dB) and the modest microwave power available at the FEL input, the power output of the harmonics is not high. However, the theory shows that one can expect substantial harmonic output if the FEL amplifier is operated so that the input microwave signal becomes nearly saturated at the output.

ACKNOWLEDGMENT

This research was supported by the Office of Naval Research.

[1] Y.-P. Chou and T. C. Marshall, Nucl. Instrum. Methods Phys. Res. A 318, 528 (1992).
[2] P. G. O'Shea *et al.*, Nucl. Instrum. Methods Phys. Res. A 341, 7 (1994).
[3] N. Piovella *et al.*, Phys. Rev. Lett. 72, 88 (1994).
[4] E. Sternbach and H. Ghalila, Nucl. Instrum. Methods Phys. Res. A 304, 691 (1991).
[5] Y.-H. Liu and T. C. Marshall, Nucl. Instrum. Methods Phys. Res. A 375, 589 (1996).
[6] Y.-H. Liu and T. C. Marshall, in *Proceedings of hte 11th International Conference on High Power Particle Beams*, Prague, 1996, edited by K. Jungwirth and J. Ullschmied (Czech Academy of Sciences, Prague, 1996), Vol. I, p. 397.
[7] C. Wang, J. L. Hirshfield, and A. K. Ganguly, Phys. Rev. Lett. 77, 3819 (1996).
[8] S. C. Chen and T. C. Marshall, IEEE J. Quantum Electron. 21, 924 (1985).
[9] S. Y. Cai, A. Bhattacharjee, and T. C. Marshall, IEEE J. Quantum Electron. 23, 1651 (1987).
[10] J. A. Pasour and S. P. Schlesinger, Rev. Sci. Instrum. 48, 1355 (1977).
[11] A. K. Ganguly and J. L. Hirshfield, Phys. Rev. E 47, 4364 (1993).
[12] H. P. Freund and T. M. Antonsen, Jr., *Principles of Free Electron Lasers* 2nd ed. (Chapman and Hall, London, 1996), Chap. 5.
[13] H. P. Freund (private communication).